GEOCHEMISTRY, GEOCHRONOLOGY, AND TECTONIC SETTING OF THE CRETACEOUS VOLCANIC ROCKS IN EAST MONGOLIA

Amarjargal Bars[1,2], Khasmaral Togtokh [1,2], Laicheng Miao[1], Fochin Zhang[1],
Munkhtsengel Baatar[3], Chimedtseren Anaad[3]

[1]*Institute of Geology and Geophysics, Chinese Academy of Sciences, Beijing 100029, China*
[2]*University of Chinese Academy of Sciences, Beijing 100049, China*
[3]*School of Geology and Mining, Mongolian University of Science and Technology, Ulaanbaatar 120646, Mongolia*

ABSTRACT

Late Mesozoic volcanic rocks in East Mongolia exhibit high-K calc-alkaline and shoshonitic series and display features of bimodal-like volcanic with a mafic and felsic members. The mafic member is composed mainly of trachybasalt and basaltic trachyandesite, with a minor amount of trachyandesite. The mafic rocks have elevated incompatible trace element concentrations and significantly negative Nb-Ta and Ti anomalies, features of typical subduction-related magmas, distinguished from OIBs. The mafic magmas have undergone fractional crystallization dominated by pyroxene and/or olivine and crustal contamination. The mafic magma was derived from low-degree partial melting of an enriched lithospheric mantle source that might have been metasomatized by subduction-derived fluids. The felsic member consists of trachydacite and rhyolite. The geochemical data indicate they produced from partial melting of a crustal source that is dominated by juvenile mafic rocks. Our new K-Ar dating and previous age data demonstrated that the late Mesozoic volcanism in East Mongolia took place during Late Jurassic-Early Cretaceous at between 156-99 Ma. The model of the arc–back-arc extension possibly induced by slab roll-back of the westward (paleo) Pacific-subduction can explain the geodynamic setting and the eastward young trend of the late Mesozoic volcanism in East Mongolia and its adjacent NE China.

Keywords: East Mongolia; late Mesozoic volcanic rock; Paleo-Pacific subduction; Mongol-Okhotsk suture

*Corresponding author. Tel.: +976-9924 9269

E-mail address: *aagii_8515@yahoo.com*.

1. Introduction

In NE Asia, Late Mesozoic volcanic rocks are mainly distributed in Eastern Central Asian Orogenic Belt (CAOB), which includes areas of Russian Far East, eastern side of NE China, Great Xing'an Range and East Mongolia (Fig. 1). The Sikhote-Alin terrane in Russian Far East is a typical subduction-accretionary complex produced by the western Pacific subduction beneath the NE Asian continent. This terrane consists of accretionary prisms, turbidites, and island arc formations. The accretionary prisms are Jurassic and early Cretaceous in age, but the arc formations are mainly Early Cretaceous, which are considered to be a result of subduction of the Paleo-Pacific (Grebennikov et al., 2016). Jahn et al. (2015) suggested that the Sikhote-Alin terrane was tectonically emplaced in two major periods: Early Cretaceous (132-98 Ma) and Eocene (46-45 Ma).

Compared with the late Mesozoic volcanic rocks along the eastern margin of the NE Asian continent (e.g. Russian Far East and east of NE China), those in East Mongolia and Great Xing'an Range are spatially distributed relatively far west from the continental margin,

meaning that they are in the interior of the continent. This leads to intensive debates regarding the origin and geodynamic setting of the volcanism. The models proposed for this include: (1) mantle plume hypothesis (Kojima, 1989; Zhou, Y et al., 2011); (2) back-arc lithosphere extension due to roll back of the subduction of Paleo-Pacific plate (Faure and Natal'in, 1992; Li and Shu, 2002; Zhang et al., 2011; Sun et al., 2013); (3) Post-orogenic diffuse extension following the subduction of Mongol-Okhotsk Ocean (Fan et al., 2003; Guo et al., 2010; Zhou et al., 2011; Li et al., 2014); and (4) westward subduction of the Paleo-Pacific Oceanic plate, leading to large scale delamination (Wu, G et al., 2005; Wang et al., 2006; Zhang et al., 2010;; Guo et al., 2013; Miao et al., 2015).

East Mongolia constitutes the westmost part of the vast late Mesozoic volcanic province in NE Asia. Contrasting to well-studied late Mesozoic volcanic rocks in NE China, those in East Mongolia are poorly-investigated. The Mongolian volcanic rocks were mapped as Cretaceous in age (Geological Map of Mongolia; 1:500 000 scale), but this age assignment lacks support of reliable age data and is also different from those in NE China, where the volcanic rocks are considered to be late Jurassic to early Cretaceous in age (Fan et al., 2003; Wang et al., 2006; Zhang L.C., et al., 2008). On the other hand, geochemical data of the Mongolian volcanic rocks are considerably limited although four possible models have been suggested for the Cretaceous volcanism in East Mongolia, including: (1) bi-directional delamination of a previously thickened mantle lithosphere, (2) back-arc extension due to collapse of a flat subduction slab, and (3) mantle avalanche of a thick pile of trapped cold mantle materials from the subducted Paleo-Asian oceanic plate (Dash et al., 2013); and (4) the stretching and breakoff of the subducted Mongol-Okhotsk oceanic slab, conjunction with gravitational collapse and spreading, as driver for late Mesozoic extension tectonism in the north China-Mongolian tract (Meng, 2003). These discrepancies give rise to the question: Did the late Mesozoic volcanic rocks in East Mongolia and NE China formed simultaneously under same geodynamic setting?

This paper presents new geochronological and geochemical data of the late Mesozoic volcanic rocks in East Mongolia, with aims: (1) to determine the eruption age of the volcanic rocks, (2) to discuss the petrogenesis of the rocks, and (3) to constrain the geodynamic setting in which they formed.

2. Geology

Eastern Mongolia and its adjacent northeastern (NE) China is an area that has been affected by at least three orogenic systems: the Central Asian Orogenic Belt (CAOB), the Mongol-Okhotsk orogenic belt and the Pacific subduction beneath the East Asian continent. The CAOB resulted from closure of the Paleo-Asian Ocean between the Siberian (-Baltica) craton in the north and North China (-Tarim) craton (NCC) in the south (Fig. 1a) at about the end of Permian to the earliest Triassic (Şengör et al., 1993; Şengör and Natal'in, 1996; Maruyama et al., 1997; Xiao et al., 2003; Miao et al., 2008). The CAOB is also considered as the largest region of Phanerozoic crustal growth in the world (Jahn et al., 2000, 2004, 2009; Safonova et al., Zhan 2015; Windley et al., 2007; Xiao et al., 2010).
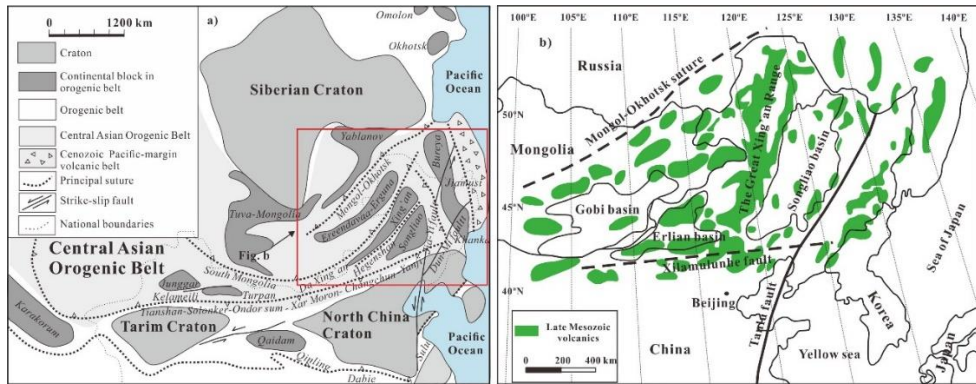
Fig. 1. (a) Simplified tectonic sketch map showing the main units of the central and eastern Asia (modified after Ge et al., 2015); (b) Distribution of late Mesozoic volcanic rocks in eastern CAOB (modified after Meng, 2003).

The Mongol-Okhotsk Orogenic Belt occurs to the north of the East Mongolia and NE China. The Mongol-Okhotsk suture, which extends for >3000 km from the central Mongolia in the west to Uda Golf in the east and possibly continues further east into the Sea of Okhotsk, is a result of closure of the Mongol-Okhotsk Ocean during late Mesozoic (Kravchinsky et al., 2002; Dong et al., 2014). Subduction of the Mongol-Okhotsk Ocean plate was traced to late Devonian as indicated by the Devonian-Carboniferous Onon arc (Zorin, 1999), but the intensive arc-magmatic activities took place during Permian to Late Triassic (Donskaya et al., 2013). Additionally, the subduction of the Mongol-Okhotsk oceanic plate was likely characterized by two-side subduction, that is, it subducted northwestward beneath the Siberian craton and southeastward beneath the East Mongolia-NE China, leading to the formations of the Khangai and Middle Gobi Permian-Triassic volcanic-plutonic belts, which are located in the southeastern and northwestern margins of the two blocks (Zorin, 1999; Van der Voo et al., 1999; Badarch et al., 2002; Kravchinskyet al., 2002; Donskaya et al., 2012), respectively. Studies have shown that the closure of the Mongol-Okhotsk Ocean was characterized by a resistor-shape pattern,

meaning that it closed earlier in its western segment (e.g. Mongolia) during Early to Middle Jurassic (Zorin, 1999; Dong et al., 2014) but in its eastern part (e.g. Russian Far East) during Late Jurassic – Early Cretaceous (Kravchinsky et al., 2002; Cogné et al., 2005).

The Pacific subduction beneath the East Asia continent has been presumed to begin from Triassic (the Paleo-Pacific), and the Sikhote-Alin terrene is considered as a result of the subduction and/or accretion system (Kojima, 1989; Zhou et al., 2014). The late Mesozoic large-scale magmatism along the eastern margin of the East Asia continent is considered to generate under the subduction setting (Zhao et al., 1989; Wu, G et al., 2005; Li and Li, 2007; Zhang, J.H et al., 2008; Safonova et al., 2009; Niu et al., 2015).

East Mongolia and NE China, which are located in the eastern segment of the CAOB between the Siberia and North China cratons, have long been considered to be composed of a series of microcontinental blocks bounded or separated by sutures and/or subduction-accretionary complexes (Şengör et al., 1993; Xiao et al., 2003). The microcontinental blocks include, from north to south, Ereendavaa-Erguna, Idermeg-Xing'an, South Mongolia-Songliao and Jiamusi-Xingkai blocks (Fig. 1a;

Zhou et al., 2009, 2011a; Liu et al., 2016). The former three blocks generally extends in NEE-SWW or NE-SW direction, whereas the last one in N-S direction in the eastern margin of the CAOB (Zhou et al., 2011). The boundaries or sutures among these blocks have been inferred to be the Mongol-Okhotsk, Xinlin-Xiguitu (the middle Gobi in Mongolian segment), Hegenshan-Heihe, Solunker-

Xilamurun and Mudanjiang sutures/faults (Fig. 1a). However, recent studies confirmed that most of these blocks are actually not microcontinents, but Phanerozoic subduction-accretionary complexes that have been metamorphosed during subduction or collision (Miao et al., 2004, 2007, 2015).
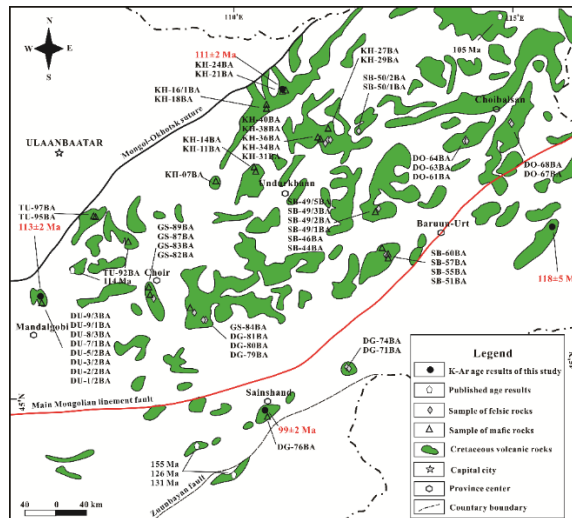
Fig. 2. Simplified map showing the distribution of late Mesozoic volcanic rocks in East Mongolia (after Tomurtogoo et al., 2012). The marked ages of late Mesozoic volcanic rocks in East Mongolia are referenced from Graham et al. (2001), Dash et al. (2013). Also shown sample locations and K-Ar ages results of this study.

Published geochronological data show that late Mesozoic volcanic rocks in NE China mainly formed during four periods of time: 163~160 Ma, 147~140 Ma, 125~120 Ma and 116~113 Ma. The volcanism appears to migrate from west to east with time (Wang et al., 2006; Zhang et al., 2010; Wu et al., 2011). On the other hand, the Mesozoic volcanism is generally coeval with, or slightly younger than, the final closure of the Mongol-Okhotsk Ocean between 160 Ma and 110 Ma (Zhang, J.H et al., 2008). Geochemical data suggest that the volcanic rocks are dominated by High-K calc-alkaline series, with rock compositions ranging from mafic to felsic (Yarmolyuk et al., 2015).

In East Mongolia, late Mesozoic volcanic rocks cover Paleozoic accretionary complexes and turbidities of the CAOB (Badarch et al., 2002). In East Mongolia and NE China, major extensional sedimentary-volcanic basins began developing during the late Mesozoic time, including the Erlian, Hailar and Songliao basins in NE China, and the East Gobi basin in the southeastern Mongolia (Wang et al., 2006). The volcanic interlayer of the Sharilyn Fm. from boreholes at the lower part of the East Gobi basin yielded an Ar-Ar age of 155±1 Ma, and Ar-Ar ages of 126±1 Ma and 131±1 have been reported for the Tsagaantsav Fm. (Graham et al., 2001). Two whole-rock Ar-Ar ages of ca. 114 and 105 Ma were reported for

the basalts in the Tsagaandelger and Dychgol areas (Dash et al., 2013), respectively. Volcanic rocks in the Erlian basin have Ar-Ar and K-Ar ages from 156 to 145 Ma (Chen and Chen, 1997; Meng, 2003) whereas those from the Hailar basin have zircon U-Pb ages of ca. 136-125 Ma (Li et al., 2014). These data suggest that the volcanic rocks were formed during the late Jurassic–early Cretaceous time.

3. Sampling and petrography

A total of 60 fresh samples were collected from outcrops at seven different provinces in East Mongolia. The localities of the samples are shown in Fig. 2. Among them, 4 samples were selected for K-Ar dating and 56 samples for geochemical analysis. Based on field observation, the late Mesozoic volcanic rocks in East Mongolia can be generally divided into two groups: a mafic group and a felsic one. The mafic rocks consist of trachybasalt, basaltic trachyandesites and trachyandesite.

Trachybasalts (samples DU-1/1BA to DU-9/3BA, KH-18BA, KH-24BA and TU-97BA) show porphyritic and intergranular or intersertal textures (Fig. 3a-b). The phenocrysts are mainly plagioclase, with pyroxene and magnetite phenocrysts occasionally observed. Polysynthetic twining and zoning are common in plagioclase phenocrysts and Glomerophenocrysts of plagioclase are also observed (Fig. 3a). The phenocrysts of pyroxene were weakly altered to be epidote and chlorite. The groundmass is composed of pyroxene, plagioclase and/or olivine. Olivine was altered to be iddingsite. Additionally, amygdaloidal and crystals of magnetites were observed in some samples (Fig. 3b).

Trachyandesites (samples; KH-21BA, SB-51BA and DG-81BA) are massive and show a porphyritic texture (Fig. 3c-e). The phenocrysts are plagioclase (Fig. 3c) and the groundmass is aphanitic containing very tiny platy plagioclase. Some phenocrysts have darkish rims (Fig. 3e), likely indicating a mineral-melt reaction.

Basaltic trachyandesites (samples KH-07BA, KH-11BA, KH-14BA, KH-16/1BA, KH-27BA, KH-31BA, KH-34BA, KH-39BA, SB-42BA, SB-44BA, SB-46BA, SB-55BA, SB-57BA, DG-76BA, GS-82BA, GS-87BA, GS-89, TU-92BA and TU-95BA) show vesicular and massive structures (Fig. 3f-h), with variable textures, such as porphyritic, intergranular or intersertal (Fig. 3g-h) and aphyric textures (Fig. 3f). It comprises plagioclase and pyroxene phenocrysts, as well as minor olivine (Fig. 3g-h). Phenocrysts of pyroxene are in irregular shape and intensively altered to be sericite and iddingsite. The groundmass is microcrystalline to aphanitic and consists of plagioclase, pyroxene, magnetite and volcanic glass, with a minor amount of secondary epidote and iddingsite. Moreover, amygdaloidal and crystals of magnetite were observed in some samples.

The felsic rocks consist of trachydacite and rhyolite. Trachydacites (samples KH-36BA, KH-38BA, KH-40BA, SB-50/1BA, SB-50/2BA, SB-60BA, DO-63BA, DG-78BA, DG-79BA and DO-67BA) are vesicle-free and display flow structure, which is indicated by the orientation of plagioclase. The trachydacites show conspicuous porphyritic and trachytic textures. The phenocrysts are plagioclase, orthoclase, biotite, hornblende and K-feldspar (Fig. 3i-l). Some K-feldspar phenocrysts have rims showing strong argillization (Fig. 3i).
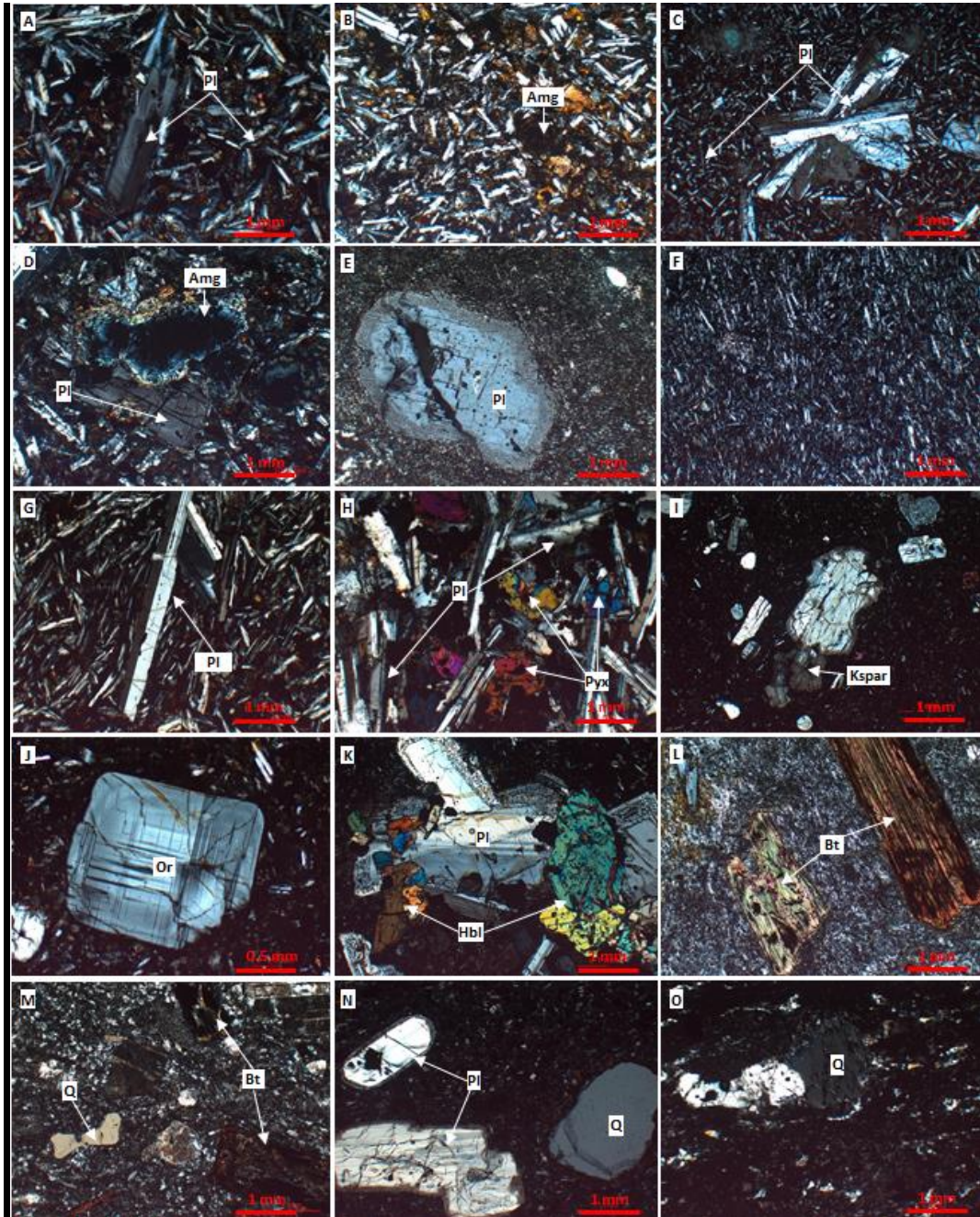
Fig. 3. Micrographphotos of late Mesozoic volcanic rocks in East Mongolia (Cross polarized light). A-B: Trachybasalts (DU1/2BA and DU-3/2BA); C-E: Trachyandesite (KH-21BA and SB-51BA); F-H: Basaltic trachyandesite (KH-14BA; GS-87BA and TU-95BA); I-L: Trachydacite (SB-60BA and DO-63BA); M-O: Rhyolite (SB-49/5BA; DO-68BA and DG-80BA). Mineral abbreviations: Px–pyroxene; Pl– plagioclase; Q– quartz; Bt– biotite; Kspar- K-feldspar; Or- orthoclase; Hbl- Hornblende; Amg– amygdaloidal.

Plagioclase phenocrysts locally have K-feldspar rims (Fig. 3k), likely a result of interaction between plagioclase and magma. Biotite was partially replaced by chlorite and hematite (Fig. 3l). The groundmass is composed of orthoclase, plagioclase and volcanic glass, with plagioclase locally altered to be epidote.

Rhyolites (samples SB49/1BA-SB-49/5BA, DO-61BA, DO-64BA, DO-68BA, DO-69BA, DG-71BA, DG-74BA, DG-80BA, GS-83BA and GS-84BA) have massive and flow structures and a typical porphyritic texture (Fig. 3m-o). Phenocrysts are plagioclase, biotite, and quartz. Plagioclase was strongly altered by argillization, and biotite was mostly altered with separation of Fe-oxides (Fig. 3m). Plagioclase shows narrow darkish rim (Fig. 3n), similarly indicating a mineral-melt reaction. Quartz is irregular in shape and shows features of re-melting (Fig. 3m-o). The groundmass is aphanitic but tiny feldspar and quartz can be observed.

4. Analytical methods

4.1. Whole-rock K-Ar dating

Whole-rock K-Ar dating was carried out at the State Key Laboratory of Earthquake Dynamics, Institute of Geology, China Earthquake Administration. The groundmass of the volcanic rocks was chosen for K-Ar dating because phenocrysts (olivine, pyroxene, and plagioclase) could be crystallized earlier in the magma chamber and thus enriched in excess radiogenic Ar. The dated rock samples were firstly crushed and sieved through 0.5-0.25 mm, purified by hand-picking under a binocular microscope (avoid from mantle xenoliths and amygdule minerals, if any), held in 5% HNO_3 for 10-15 minutes, and washed with distilled water.

Potassium and argon were measured on two separated aliquots of the selected grains. Potassium concentration was measured by the flame spectrophotometry using optimized analytical conditions and the uncertainty is 1.0-1.5%. The Ar isotopes were determined on the MM1200 mass spectrometer, and the MM1200 mass spectrometer was connected with the whole metal extraction system and purification system. An extraction system for internal and external double vacuum system, using beam furnace heating in a vacuum system including tube and purification system and the mass spectrometer is communicated with the vacuum system for the electron bombardment, precise temperature control by using the compensation method, the error is ±5ºC. The sample was loaded into the sample tube and was heated for 12 hours or more at 250ºC. Each sample was put with molybdenum tantalum lining clamp pot, heating under bombardment electronic vacuum system. The gas releases through a cold trap to remove water and CO_2, and through the titanium sponge to remove other reactive gasses, and finally through the Zr-Al third level getter purification. The purified inert gas was introduced into the mass spectrometer MM1200 for analyses. Decay constants are those recommended by the ISG (Steiger and Jäger, 1977): $\lambda=5.543\times10^{-10}$/yr, $\lambda_e=0.581\times10^{-10}$/yr, and $\lambda_\beta=4.962\times10^{-10}$/yr.

4.2. Major and trace elements

Samples for geochemical analysis were crushed to mm-scale fragments after removal of altered rims. The rock fragments were washed in distilled water in an ultrasonic bath and further crushed in a WC jaw crusher. An aliquot of the cleaned material was ground in an agate ring mill to <200 mesh, and the resulting powder used for major and trace element analyses. Both the major and trace element analyses were conducted at the Institute of Geology and Geophysics, Chinese Academy of Sciences (IGGCAS). Major element oxides were determined by X-ray fluorescence (XRF) spectrometer. Detailed

analytical processes and conditions are same as described by Guo et al. (2006). Loss on ignition (LOI) was determined by weighing about 0.5g powder samples baked at 1000ºC for 1h. For trace element analysis, the powder samples were digested in a mixture of HF and HNO_3 in high-pressure Teflon bombs for 7 days. The solutions were analyzed using an Inductively Coupled Plasma Mass Spectrometry (ICP-MS), and analytical error for most elements is less than 5%. The accuracy was based on the analyses of standards GSR1 and GSR3. Detailed ICP-MS analytical procedures follow those described by Li et al. (2009).

5. Results

5.1. K-Ar dating

K-Ar dating results of 4 samples are presented in Table 1 and are shown in Fig. 2. Two trachybasalt samples (DU-1/1BA and KH-25BA) yielded ages of 113±2 and 111±2 Ma, respectively. The basaltic trachyandesite sample (DG-75BA) gave an age of 99±2 Ma, and the rhyolite sample (DO-70BA) yielded an age of 118±5 Ma. These ages are interpreted to represent the eruption times of the volcanic rocks.

Table.1. K-Ar whole-rock dating results of late Mesozoic volcanic rocks in East Mongolia.

Sample name	Province	Coordinate		K (%)	^{40}Ar rad	^{40}Ar rad (%)	±1σ, Ma
DU-1/1BA	Dundgobi	E106.42°	N46.15°	1.87	3.7995E-10	96.87	113±2
KH-25BA	Khentii	E 110.76°	N48.55°	1.87	3.7015E-10	95.45	111±2
DO-70BA	Dornod	E 115.18°	N46.60°	0.16	3.3731E-11	53.77	118±5
DG-75BA	Dornogobi	E 110.09°	N44.78°	2.16	3.8271E-10	91.74	99±2

5.2. Major and trace elements

Analytical results of major and trace elements are listed in Table 2. In total alkali (Na_2O+K_2O) vs. SiO_2 plot (Fig. 4a) in the fields of trachybasalt, trachyandesite, basaltic trachyandesite, trachydacite and rhyolite, mostly belonging to alkaline series. In K_2O vs. SiO_2 diagram, the Mongolian volcanic rocks belong to the high-K calc-alkaline to shoshonitic series (Fig. 4b). From the Harker variation diagrams (Fig. 5), it is evident that most oxides (e. g. TiO_2, Al_2O_3, MgO, MnO and P_2O_5) of the volcanic rocks have no linear correlations with SiO_2, but they do from basaltic to intermediate (called "mafic group" hereafter) and from dacitic to rhyolitic magmas (called "felsic group" hereafter), respectively.

The mafic group volcanic rocks have SiO_2 contents of 49.74-59.89 wt.%, with high Al_2O_3 (14.26-17.38 wt.%). They have MgO contents varying from 1.96 to 5.45 wt.%, K_2O contents ranging from 1.32 to 3.74 wt.% and K_2O/Na_2O ratios from 0.36 to 0.97 wt.%. The volcanic rocks of the felsic group have high SiO_2 contents (63.47-75.69 wt.%) and high K_2O contents (3.25-5.68 wt.%). Their MgO contents range from 0.11 to 1.54 wt.%. They have high total alkali contents ranging from 7.45 to 10.12 wt.%, with relatively high K_2O/Na_2O ratios of 0.66-2.54, consistent with high-K calc-alkaline and shoshonitic rocks. Both the mafic and the felsic group rocks have relatively low Mg# $[=Fe^{2+}/(Fe^{2+}+Mg)*100]$ values, ranging from 27.76 to 59.37 and from to 10.73 to 49.86, respectively (Table 2). LOI values of volcanic rocks have been considered as indicators of the presence of hydrous mineral phases (e.g., amphibole) and/or secondary minerals (e.g., chlorite and carbonate). The LOI values of the East Mongolian samples of both mafic and felsic groups are variable (0.22-3.84 wt.%), but show no correlation with La/Sm ratios, suggesting that alteration did not create significant

modification on REE patterns (Labanieh et al., 2012).
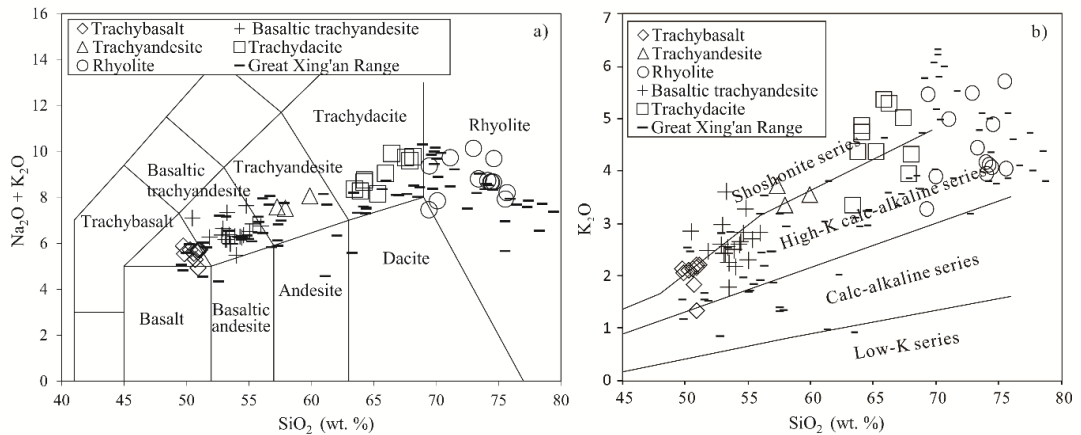
Fig. 4. (a) TAS classification diagram ($Na_2O + K_2O$ vs. SiO_2; after Maitre et al., 1989) and (b) K_2O vs. SiO_2 diagram (after Peccerillo and Taylor, 1976) for late Mesozoic volcanic rocks in East Mongolia. Data of the Great Xing'an Range are referred from literature Fan et al. (2003), Meng et al. (2011), Yu et al. (2014) and Li et al. (2015).

The $\sum$REE contents of the volcanic rocks of the mafic group range from 149 to 571 and those of the felsic group from 120 to 470. The two groups have similar chondrite-normalized rare earth element (REE) patterns characterized by enrichment in light rare earth elements (LREEs) relative to heavy rare earth elements (HREEs), with $(La/Yb)_{CN}$ ratios of 15.72-43.87 and 7.59-25.8 respectively, except for that the felsic group rocks have stronger negative Eu anomalies than the mafic group (Fig. 6a, c). The volcanic rocks of the mafic group have slightly higher $(Gd/Yb)_{CN}$ ratios-ranging from 2.9 to 6.71 than those of the felsic group, which vary from 1.12 to 3.41 (Fig. 6a, c). Trace element concentrations range from several times primitive mantle for heavy REE and Ti to several hundred times for LILEs, such as Rb, Ba, Th and U (Fig. 6b, d). In the primitive mantle (PM)-normalized trace element diagrams, the East Mongolian volcanic rocks display enrichment in large ion lithophile elements (LILEs), such as Ba and Rb, but depletion in high field strength elements (HFSEs, e.g. Nb and Ta) relative to Th and La. Comparing with the mafic group, the felsic group shows more distinguished negative Eu, Sr, and Ti anomalies, with variable Ba anomalies (Fig. 6b, d).
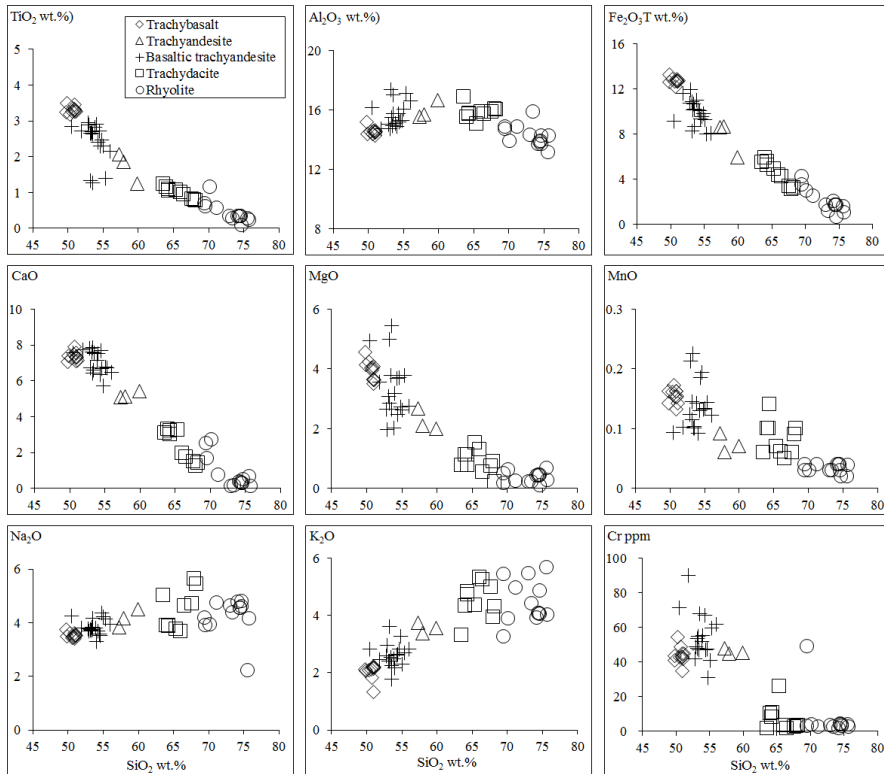
Fig. 5. Harker diagrams showing the co-variation of major oxides with SiO₂ for the late Mesozoic volcanic rocks in East Mongolia.
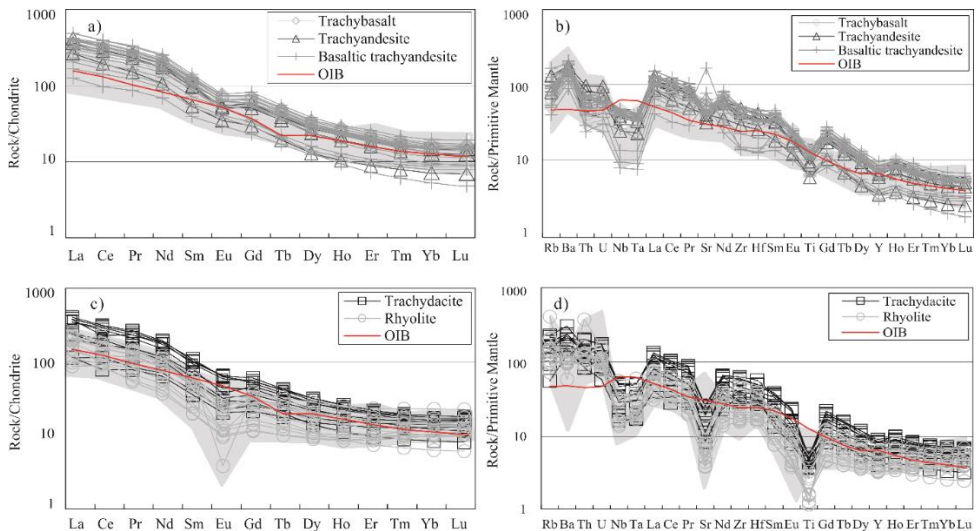
Fig. 6. Chondrite-normalized REE patterns and Primitive mantle-normalized trace element spiderdiagrams for the late Mesozoic volcanic rocks in East Mongolia. Figures a and b are mafic volcanic rocks; figures c and d are felsic volcanic rocks. The volcanic rocks of the Great Xing'an Range, NE China, are also shown in gray shadow for comparisons and the data sources are same as those in Fig. 4. The normalized values of both the chondrite and the primitive mantle are after Sun and McDonough (1989).

6. Discussion

6.1. Eruption time of the late Mesozoic volcanic rocks in East Mongolia

In East Mongolian, the late Mesozoic volcanic rocks were ascribed to be the Early Cretaceous of age on the 1:500,000 Geological Map of Mongolia (Institute of Geology, Ministry of Heavy industry of Mongolia, 1990), but this assignment lacks support from isotopic age data. Our new K-Ar dating results demonstrate that the dated volcanic rocks were mainly formed during early Cretaceous (118-99 Ma). In combination with previously published and age data aforementioned, it can be concluded that the late Mesozoic volcanic rocks in East Mongolia likely erupted between 155 and 99 Ma, belonging to Late Jurassic to Early Cretaceous. These data attest that the Mesozoic volcanic rocks in East Mongolia are essentially coeval with those in the Great Xing'an Range, NE China (160-100 Ma; Davis et al., 2001; Wang et al., 2006; Ying et al., 2010;), but appear some older than those in the areas of farther east, such as the Songliao Basin (140-106 Ma; Wang et al., 2002; Zhang, H.F et al., 2007; Shu et al., 2007; Ding et al., 2007; Gao, 2008), Jiamusi (130-80 Ma; Yu et al., 2009; Xu et al., 2013), Russian Far-East (132-80 Ma; Cogne et al., 2005; Jahn et al., 2015), the southern Korean Peninsula (110-70 Ma; Kim et al., 2012, 2014; Koh et al.,2013; Kihm et al., 2014) and the southwestern Japan (95-65 Ma; Li et at., 2007; Sato et al., 2016). Generally, the late Mesozoic volcanism in NE Asia displays a decreasing trend of eruption ages from East Mongolia in the west to Japan in the east (Fig. 7). This temporal and spatial variation possibly implies that the subduction zone of the western Pacific plate migrated from west to east or a slab roll-back of the subducted plate (see section 6.3 for details).
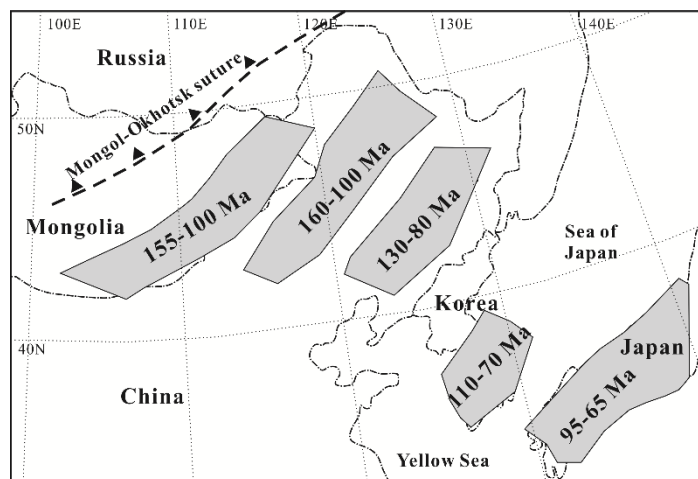
Fig. 7. A sketch showing the spatial and temporal variations of the late Mesozoic volcanism in NE Asia, which appears that an eastward migration from East Mongolia – Greater Xing'an Range to the southwestern Japan existed (after Wang et al., 2006; age data are from Shuvalov, 1980, 1982; Graham et al., 2001; Dash et al., 2013; Zhao et al., 1989; Davis et al., 2001; Fan et al., 2003; Meng, 2003; Wang et al., 2006; Chen et al., 2007; Guo et al., 2008; Zhang, J.H et al., 2008, 2010; Ying et al., 2010; Xu et al., 2013; Li et al., 2014; Wang et al., 2002; Zhang, H.F et al., 2007; Shu et al., 2007; Ding et al., 2007; Gao, 2008; Yu et al., 2009; Xu et al., 2013; Cogne et al., 2005; Jahn et al., 2015; Li et at., 2007; Sato et al., 2016).

6.2. Petrogenesis of the late Mesozoic volcanic rocks in East Mongolia

As aforementioned, there are no linear correlations of most oxides with SiO_2 between the mafic and felsic groups of volcanic rocks (Fig. 5). This indicates that the rocks of the two groups were probably derived from different source regions. The relatively high LOI contents of the mafic samples (0.22–3.84 wt.%; Table 2) indicate that the mafic rocks experienced variable alternations during post-eruption processes. This is further supported by our thin section observation that widespread epidotization and chloritization occurred in the basaltic rocks. The post-eruption alteration may have changed the contents of some incompatible elements (e.g. LILEs) due to their high mobilities. Therefore, relatively stable elements (e.g. HFSEs and REEs) are used to constrain the original geochemical characteristics of the magmas in the following discussion.

6.2.1. Petrogenesis of the mafic volcanic rocks

The Mongolian mafic group rocks may have experienced some fractional crystallization and crustal contamination during the magma ascent from its mantle source. The mafic rocks show low Mg# values of 27.76 to 59.37 and low Cr concentrations (31-155.95), and MgO and Cr are negatively correlated with SiO_2 (Fig. 5), indicating that the magma of the mafic group rocks are not primitive and likely experienced some fractional crystallization of pyroxene, most likely of clinopyroxene (Cpx) and olivine. Slightly negative Eu anomaly suggests that fractionation of plagioclase and Cpx contributes little to the petrogenesis of the mafic group rocks. This is consistent with the observation that Cpx and plagioclase are the dominant phenocrysts in the rocks. The fractional crystallization trend in La/Yb vs. Yb plot (Fig. 8a) also confirms that the mafic group rocks experienced fractional crystallization. The mafic group rocks are enriched in Th (2.1-8.93 ppm), and there is a good positive correlation between Nb/Th and Nb/La (Fig. 8b), suggesting that a Th-enrich component involved in their petrogenesis, which is most likely due to crustal contamination (Li et al., 2006; Yang et al., 2016). Studies have shown that continental crust is typically depleted in Nb and Ta (Rudnick and Fountain, 1995), and the upper continental crust is enriched in La and Th whereas the lower continental crust is not always enriched in Th (Barth et al., 2000). In the $(Th/Ta)_N$ vs. $(La/Ta)_N$ plot, the Mongolian mafic samples define an UCC trend (Fig. 9a; Ingle et al., 2002), implying that the contaminator is the upper continental crust. In addition, the La/Ba vs. La/Nb diagram (Fig. 9b) also shows that crustal contamination has a major contribution to the petrogenesis of the mafic group rocks.
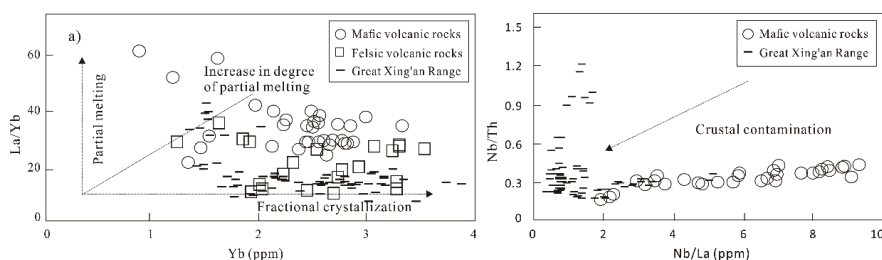
Fig. 8. (a) La/Yb vs. Yb diagram (after Zhu et al., 2009) showing fractional crystallization of the volcanic rocks in East Mongolia (the Great Xing'an data are same as in Fig. 4); (b) Nb/Th vs. Nb/La plot showing the crustal contamination of the mafic rocks.
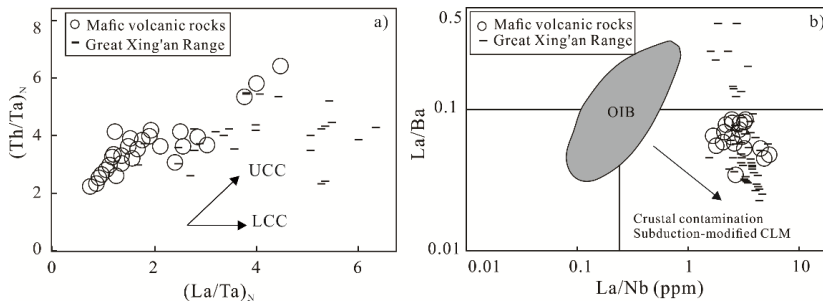
Fig. 9. (a) (Th/Ta)$_N$ vs. (La/Ta)$_N$ and (b) La/Ba vs. La/Nb (after Thirlwall et al., 1994) diagrams for late Mesozoic mafic volcanic rocks in East Mongolia (The data are same as in Fig. 4).

The volcanic rocks of the mafic group, which belong to high-K calk-alkaline to shoshonitic series (Fig. 5), have considerable high REE contents (from 149 to 571 ppm) and OIB-like REE patterns (Fig. 6a, c) reminiscent of OIBs. However, they display distinct negative anomalies of HFSEs (e.g. Nb, Ta, and Ti) in the primitive mantle-normalized diagram (Fig. 6b, d), a feature characteristic of subduction-related magmas (Yang et al., 2014). Presented geochemical data define the Mongolian mafic volcanic rocks deriving from a subcontinental lithospheric mantle source (Fig. 10a) that might have metasomatized by a subduction-related component (Fig. 10b).
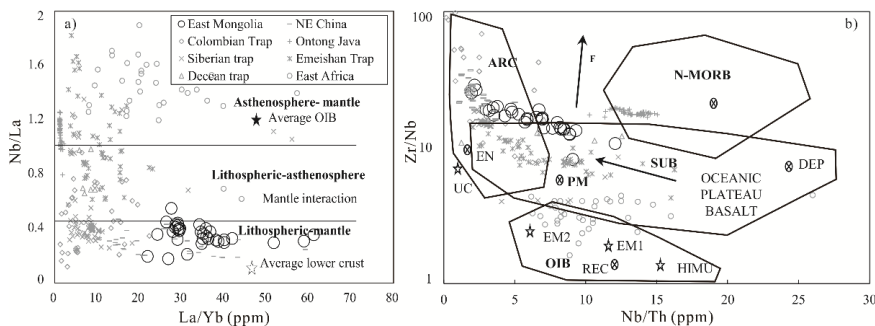
Fig. 10. Diagrams for identifying components of the mantle source of the Mongolia mafic volcanic rocks. (a) Nb/La vs. La/Yb plot (Smith et al., 1999; modified after Karsli et al., 2014). Average OIB is taken from Fitton et al. (1991); average lower crust value is an average of six granulite xenoliths from the lower crust after Chen and Arculus (1995); (b) Zr/Nb vs. Nb/Th plot (after Condie, 2005). Arrows indicate effects of batch melting (F) and subduction (SUB). UC– upper continental crust; PM– primitive mantle; DM– depleted mantle; HIMU– high U/Pb mantle; EM1– enriched mantle I; EM2– enriched mantle II; ARC– arc-related basalts; NMORB– normal ocean ridge basalt; OIB– oceanic island basalt; DEP– deeply depleted mantle; EN– enriched component; REC– recycled component. Some typical basalts in the world are also shown for comparison and the data sources are: NE China: Fan et al., 2003; Ji et al., 2007; Yu et al., 2009; Meng et al., 2011; Guo et al., 2013; Sun et al., 2013; Xu et al., 2013; Dong et al., 2014; Li, S.C et al., 2014; Li, S.Q et al., 2014; Yang et al., 2015; Columbian Trap: Nivia et al., 2006; Lara et al., 2012; Ontong Java: Fitton and Godard, 2004; White et al., 2004; Siberian Trap: Reichowa et al., 2005; Chuvashova et al., 2016; Svetlitskaya et al., 2016; Emeishan Trap: Xiao Long et al., 2003; Zi et al., 2008; Deccan Trap: Sheth et al., 2004; Duraiswami et al., 2013; East Africa: MacDonald et al, 2001).

Nb/Yb and/or Ta/Yb ratios can be used to constrain relative depletion or enrichment nature of the mantle sources of basaltic magmas if the degree of partial melting is small, even if garnet as a residual phase in the source (Pearce and Stern, 2006; Pearce et al., 2005). Meanwhile, Th/Yb ratio is considered as a sensitive indicator for monitoring addition of subduction components (Stern et al., 2003; Pearce et al., 2005; Pearce and Stern, 2006). In the Th/Yb vs. Ta/Yb diagram (Fig. 11a), the Mongolian mafic group samples plot in the field of active continental margins and straddle on the boundary between the EMORB-OIB mantle arrays. The relatively high Th/Yb ratios that cause a generally vertical deviation from

the mantle array may reflect the input of subduction components into the mantle source. Besides, relatively high Ba/Th and low La/Sm ratios (Fig. 11b) as well as the positive Ba positive anomalies (6b) of the Mongolian mafic rocks attest that the magma mantle source was predominately metasomatized by aqueous fluids derived from slab dehydration, rather than by melts of partial melting of the subducted sediments (Labanieh et al., 2012) because subduction-related fluids are generally enriched in elements such as Ba, Rb, and U but depleted in Th, Nb, Ta, Ti and REE (Brenan et al., 1995; Ayers et al., 1997; Kessel et al., 2005).
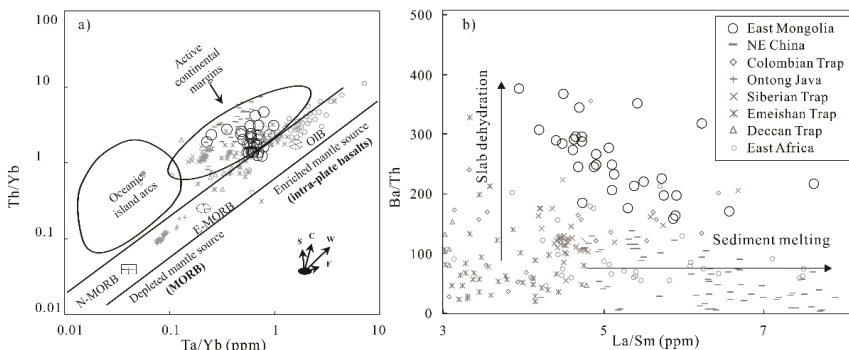
Fig. 11. (a) Th/Yb vs. Ta/Yb (Pearce, 1983) and (b) Ba/Th vs. La/Sm (Labanieh et al., 2012) plots showing the mantle source nature of the Mongolian mafic rocks (the data are same as those in Fig. 4).

It is considered that K-rich basaltic rocks are usually generated from partial melting of amphibole/phlogopite-bearing mantle rocks and their K concentrations controlled by the amphibole/phlogopite abundance and the degree of partial melting (Avanzinelli et al., 2009; Conticelli et al., 2009a, 2009b; Yang et al., 2014). Studies have shown that amphibole from mantle xenoliths has relatively high abundances of K, LREE, HFSE, and Ba but very low abundances of Rb and Th (Ionov and Hofmann, 1995; Chazot et al., 1996) and phlogopite is rich in K, Ba and Rb, but has very low concentrations of REE, HFSE and Th. The

K/Rb ratios of phlogopites vary from 40 to 400, whereas those of amphibole and amphibole-bearing melt are generally greater than 1100 (Chakrabarti et al., 2009). The mafic volcanic rocks in East Mongolia have relatively high K/Rb ratios (165-883), implying that amphibole is the dominant hydrous mineral in the mantle source. The La/Sm and La/Yb ratios of the Mongolian mafic rocks are 3.96-7.64 and 21.91-61.14, respectively, which illustrates that the Mongolian mafic volcanic rocks were produced by the batch partial melting of spinel and/or garnet peridotite (e.g., Genc and Tuysuz, 2010). In terms of the La/Sm vs. La

ratios, the partial melting curves that coincide with the compositions of the mafic volcanic

rocks imply a low-degree partial melting (<5%) of an enriched mantle source (Fig. 12).
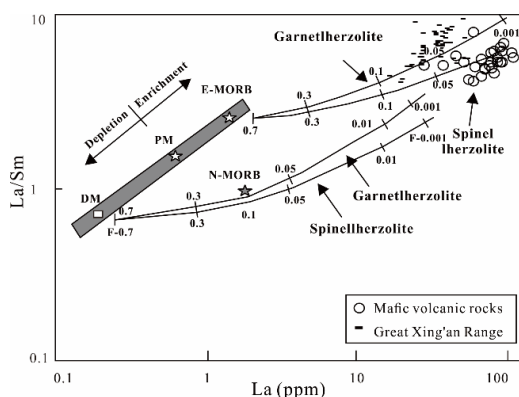
Fig. 12. La/Sm vs. La diagram (after Zhu et al., 2009) showing the source and fractionation characteristics of mafic volcanic rocks in East Mongolia.

In summary, the geochemical data demonstrate that the mafic group volcanic rocks in East Mongolia was produced by low-degree partial melting of an enriched lithospheric mantle source that is likely dominated by spinel-facies lherzolite and might have been metasomatized by subduction-related fluids, and experienced fractional crystallization dominated by the fractionation of pyroxene and/or olivine and crustal contamination possibly by upper crustal materials.

6.2.2. Petrogenesis of the felsic group volcanic rocks

It is generally accepted that direct melting of the mantle could not have produced the felsic members (Campbell et al., 2014 and references therein). Furthermore, there are no linear correlations of most major oxides contents with SiO_2 between the mafic and felsic group rocks in East Mongolia although a rough trend of decrease in Cr and MgO concentrations with increasing SiO_2 contents can be observed (Fig. 5). This precludes the possibility that the felsic group rocks were derived by fractional crystallization from the mafic group rocks. Therefore, we suggest that

the felsic group rocks in East Mongolia probably have different source regions from the associated mantle-derived mafic group volcanic rocks. This conclusion is consistent with the observation that intermediate volcanic rocks; if there is any, account for just small proportions of the volcanic sequences in East Mongolia (Figs. 4 and 5). In other words, the late Mesozoic volcanic rocks in East Mongolia actually have features of bimodal volcanic rocks in terms of lithology and geochemical composition.

The Mongolian felsic group volcanic rocks have resembled chondrite-normalized REE and PM-normalized trace element patterns to those of the mafic group rocks, but displays more evidently negative Eu, Sr and Ti anomalies and lesser distinctly positive Ba anomaly than the mafic rocks (Fig. 6, d), indicating fractional crystallization dominated by plagioclase and Ti-bearing minerals (e.g. rutile) contributes to the petrogenesis of the felsic group rocks (Fig. 6d). On the other hand, these geochemical features favor an explanation that the Mongolian felsic group rocks were originated from partial melting of a mafic crustal source. However, the uncertainty

remains as to whether juvenile or ancient mafic materials account for the mafic source of the felsic rocks. In this aspect, the Nd-Hf isotope signatures of the rhyolite in the Gehe basin in the Great Xing'an Range of NE China can give some clues because it is geographically adjacent to East Mongolia and the late Mesozoic volcanic rocks in the two areas are contemporaneous and display similar, if not identical, major and trace element geochemistry (Figs. 4, 5 and 6). In the Gehe basin, the felsic volcanic rocks have similar or overlapping Nd-Hf isotope compositons to those of associated mafic volcanic rocks, with $\varepsilon_{Nd}(t)$ and $\varepsilon_{Hf}(t)$ values of 0.86-2.12 and 2.9-3.3 (Zhang, L.C et al., 2007), respectively. The similarities in Nd-Hf isotope composition of the mafic and felsic rocks provide compelling evidence for the felsic rocks deriving from a juvenile mafic source. Consequently, we propose that the Mongolian felsic group rocks were similarly generated by low-degree partial melting of a juvenile crustal source. Underplated mafic rocks that are coeval with the exposed mafic group rocks and/or juvenile mafic materials of the CAOB; are plausible candidates for the juvenile crustal source.

6.3. Tectonic implications

It is commonly accepted that the late Mesozoic volcanic rocks in East Mongolia and NE China were formed in an extensional environment (e.g. Faure and Natal'in, 1992). The bimodal-like nature of the late Mesozoic volcanic rocks in East Mongolia complies with this cogonization. However, the tectonic mechanism that generates the extensional environment in which the volcanic rocks formed is yet an issue of debates. In this regard, several models have been proposed, mainly including mantle plume (Lin et al., 1998; Ge et al., 1999; Zhou, Y et al., 2011), post-orogenic extension or lithospheric delamination following the Mongol-Okhotsk orogenesis (Wang et al., 2002; Fan et al., 2003; Zhou et al., 2009; Zhou et al., 2011; Li et al., 2014) or the CAOB (or called lithospheric mantle avalanche model of Dash et al., 2013), and back-arc extension of the Pacific subduction (Zhao et al., 1989; Li and Shu, 2002; Zhang et al., 2011; Sun et al., 2013).

Our new geochemical and geochronological results do not support a mantle plume origin for the late Mesozoic volcanic rocks in East Mongolia. Instead, they point to an origin of subduction-related magmas (Fig. 12a), similar conclusions reached for the late Mesozoic volcanic rocks in the Great Xing'an Range (Zhang, J.H et al., 2008; Zhou et al., 2009). However, these authors selected the post-orogenic extension following closure of the Mongol-Okhotsk Ocean to interpret the geodynamic setting in which the volcanic rocks generated because they considered that their study areas are too far from the Pacific subduction to correlate the volcanism with the subduction.
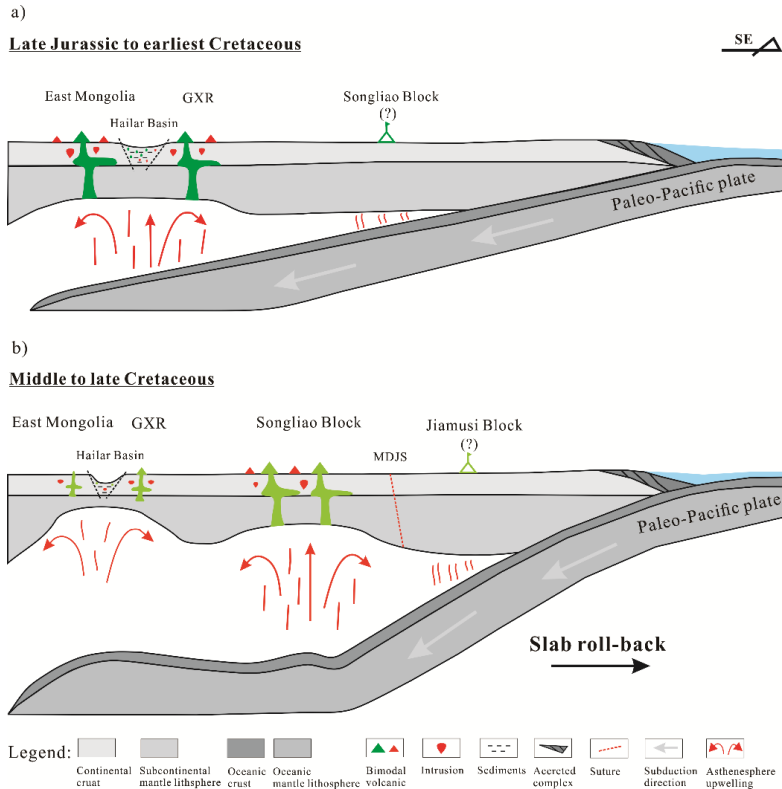
Fig. 13. Simplified tectonic model of late Mesozoic volcanic rocks in East Mongolia and Great Xing'an Range, NE China (modified after Sun et al., 2013).

Late Mesozoic volcanic rocks are distributed in a vast area, including East Mongolia, NE China, and the eastern North China craton (NCC), which would be difficult to interpret the coeval magmatism in the southern part of the NE China and eastern NCC if interpreting just in terms of post-orogenic extension of the Mongol-Okhotsk orogeny (Dash et al., 2013).

The lithospheric mantle avalanche model (Dash et al., 2013) suggests that a thick pile of subducted oceanic slabs from the Paleo-Asia oceans was trapped at the top of the endothermic phase boundary at 670 km, and the initiation of the Pacific subduction may have caused a thermal perturbation, raising the temperature and thus reducing the viscosity of the upper mantle, which in turn caused rapid sinking of the cold pile of lithosphere through the 670 km phase boundary, and mantle materials filling the gap of the slab pile caused upwelling and thus decompression melting. This model meets two challenges: one is that it cannot explain the eastward young trend of the late Mesozoic volcanism in NE Asia if the thermal perturbation was from initiation of the Pacific subduction, which will lead to a reversed age variation pattern; the other is that it lacks evidence of large-scale subducted paleo-Asian oceanic slab existing at the 670-km boundary before Cretaceous.

As a matter of fact, the late Mesozoic volcanic rocks are discontinuously distributed, and individual volcanic belts generally extend in NNE diction, parallel to the Mesozoic volcanic-sedimentary basins (e.g. the Hailar

and the Songliao basins), both of which are conformable to the Pacific subduction zone (e.g., Li, 2000; Wu et al., 2005a, b). This implies that the volcanism is likely related to the Pacific subduction. Therefore, we prefer the model of the back-arc extension induced by the westward Pacific-subduction, as suggested by Sun et al. (2013), to explain the geodynamic

7. Conclusion

1) Our new K-Ar dating results, in combination with previously published age data, demonstrate that the volcanic rocks in East Mongolia formed in late Jurassic-early Cretaceous, with eruption ages ranging from ca. 155 to 99 Ma, essentially coeval with those of its adjacent Great Xing'an Range of NE China.

2) The late Mesozoic volcanic rocks in East Mongolia are characterized by high-K calc-alkaline and shoshonitic series and displays features of a bimodal-like volcanic suite in lithology and geochemistry. The mafic rocks, which are mainly composed of trachybasalt and basaltic trachyandesite with minor trachyandesite, resulted from low-degree partial melting of the lithospheric mantle that had been metasomatized by subduction-related fluids, and experienced fractional crystallization and crustal contamination; the felsic rocks including trachydacite and rhyolite were generating from partial melting of juvenile mafic lower crust.

3) The geochemical data and the bimodal-like occurrence of the volcanic rocks in East Mongolia indicate an extension environment in which they formed. Considering evidence of adjacent NE China together, we use the model of the arc–back-arc extension, possibly induced by slab roll-back, of the westward (paleo) Pacific-subduction to explain the

setting under which the late Mesozoic volcanic rocks in East Mongolia and NE China formed. This model emphasizes that the slab roll-back of the subduction retreat of the Pacific plate might have caused the upwelling of the asthenospher, which in turn caused the extension and melting of the overriding lithosphere (Fig. 13).

geodynamic setting and the eastward young trend of the volcanism.

Table 2. Major (wt.%) and trace (ppm) elements composition for late Mesozoic volcanic rocks of East Mongolia.

Sample number	DU-1/2BA	DU-2/2BA	DU-3/2BA	DU-5/2BA	DU-7/1BA	DU-8/3BA	DU-9/1BA	DU-9/3BA	TU-97BA	KH-24BA	KH-18BA	KH-21BA	DG-81BA	SB-51BA	KH-07BA	KH-11BA	KH-27BA	KH-29BA	KH-34BA
Rock type	Trachybasalt								Trachyandesite						Basaltic trachyandesite				
Oxides (wt. %)																			
SiO2	49.85	49.03	50.11	49.61	50.01	49.85	50.15	49.74	48.81	49.42	50.16	56.11	58.72	56.93	54.84	54.15	52.89	53.39	53.44
TiO2	3.15	3.44	3.19	3.21	3.25	3.20	3.28	3.21	3.19	3.27	3.39	2.02	1.22	1.83	2.11	2.39	2.77	2.25	2.23
Al2O3	14.41	14.16	14.26	14.12	14.01	14.21	14.42	14.14	14.89	14.21	14.26	15.23	16.32	15.44	16.26	15.69	14.83	14.95	15.61
Fe2O3T	12.77	13.05	12.48	12.45	12.62	12.49	12.49	12.36	12.36	11.86	12.57	8.41	5.84	8.52	7.92	10.06	10.78	9.35	9.03
MnO	0.16	0.16	0.14	0.17	0.16	0.15	0.13	0.15	0.14	0.15	0.16	0.09	0.07	0.06	0.12	0.13	0.14	0.19	0.13
MgO	4.21	4.07	3.57	3.95	3.96	3.55	3.46	3.56	4.49	3.87	4.03	2.63	1.96	2.06	2.70	3.67	1.99	3.63	2.55
CaO	7.21	7.29	7.02	7.35	6.98	7.21	7.19	7.13	6.91	7.69	7.43	4.98	5.33	5.06	6.34	6.32	7.02	6.55	6.57
Na2O	3.58	3.43	3.46	3.36	3.35	3.40	3.47	3.44	3.68	3.38	3.54	3.75	4.42	4.08	3.85	3.67	3.74	3.45	4.09
K2O	2.08	2.02	2.15	2.09	2.16	2.10	2.17	2.13	2.09	1.77	1.31	3.67	3.48	3.31	2.76	2.60	2.45	2.76	2.24
P2O5	1.69	1.73	1.68	1.74	1.74	1.72	1.74	1.70	1.56	1.83	1.62	1.09	0.68	1.00	1.06	1.05	1.56	1.30	1.18
LOI	0.80	1.06	1.48	1.68	1.20	1.72	1.66	1.94	1.44	1.86	1.20	1.98	1.28	1.10	1.54	0.22	1.40	1.68	2.62
TOTAL	99.91	99.44	99.55	99.72	99.44	99.60	100.16	99.50	99.56	99.32	99.67	99.96	99.32	99.40	99.50	99.95	99.56	99.49	99.69
Trace elements (ppm)																			
Li	21.38	16.33	18.81	32.05	17.40	15.06	23.55	21.63	15.24	15.35	12.89	15.52	19.97	20.05	10.63	14.94	12.35	20.95	14.78
Be	2.87	2.52	2.75	2.72	2.61	2.28	2.74	2.58	2.23	2.74	2.51	3.20	2.15	3.35	2.67	2.31	2.96	3.23	2.90
Sc	17.78	16.35	16.38	16.98	16.91	15.53	17.17	16.39	14.91	15.15	15.68	12.71	8.75	13.02	15.93	16.70	16.49	14.82	12.86
V	209.20	198.25	187.73	192.02	190.07	161.20	205.11	184.60	197.2	192.13	196.71	130.30	112.11	148.85	144.04	98.13	201.91	156.06	162.46
Cr	54.33	41.13	44.88	42.90	43.20	34.95	42.49	41.70	43.55	48.68	44.97	47.88	45.24	44.72	61.84	66.92	51.77	47.61	40.78
Co	32.46	30.11	27.55	27.54	27.33	22.40	27.42	26.71	30.32	26.71	27.92	16.70	14.87	17.22	21.06	23.51	24.77	22.61	20.51
Zn	200.44	190.27	192.08	194.02	195.63	167.01	194.91	192.09	174.2	190.30	188.92	154.68	117.44	128.90	147.82	161.99	171.77	164.27	153.81
Ga	26.13	23.73	23.18	24.36	23.31	20.55	23.87	23.50	23.51	24.01	23.49	23.05	21.71	24.32	23.74	23.37	24.57	23.18	23.79
Rb	41.15	36.36	40.93	42.49	40.50	35.61	39.38	34.17	34.58	33.06	61.72	93.13	54.62	92.19	66.95	64.20	54.53	87.85	98.01
Sr	1009.8	912.20	870.93	936.92	821.28	805.69	879.07	871.68	809.0	1317.4	969.70	693.67	887.97	800.71	867.73	1018.4	920.44	827.24	938.06
Y	34.82	32.97	35.35	37.49	36.52	33.95	37.59	35.44	29.74	33.39	32.20	29.33	15.14	26.35	30.17	32.31	34.98	32.25	25.00
Zr	449.16	377.15	434.50	452.88	439.62	380.06	460.89	424.80	339.4	449.70	366.64	576.86	337.13	503.14	437.38	383.66	577.00	561.82	449.31
Nb	36.02	29.95	31.81	32.18	31.90	27.45	34.06	31.28	31.73	27.18	27.52	28.75	18.03	26.49	22.26	22.26	30.45	29.34	26.38
Cs	0.94	0.92	0.66	0.61	0.71	0.44	0.43	0.65	1.60	0.56	2.04	0.97	0.55	1.85	0.71	0.89	7.07	5.37	1.44

	DU-1/2BA	DU-2/2BA	DU-3/2BA	DU-5/2BA	DU-7/1BA	DU-8/3BA	DU-9/1BA	DU-9/3BA	TU-97BA	KH-24BA	KH-18BA	KH-21BA	DG-81BA	SB-51BA	KH-07BA	KH-11BA	KH-27BA	KH-29BA	KH-34BA
Ba	1162.8	1030.5	1114	1145.1	1075.9	968.99	1135.6	1077.9	930.3	1430.2	1103.9	1284	1210	1391.3	1103.9	1142.2	1242.5	1207.4	1190.4
La	85.72	71.70	79.74	83.68	81.72	74.18	80.89	79.76	58.67	85.68	62.52	99.87	62.62	85.78	71.47	63.77	91.45	99.15	82.65
Ce	187.37	160.48	178.75	183.28	179.75	156.88	183.13	173.65	130.1	193.38	143.76	196.32	118.59	175.98	152.58	136.19	202.06	200.23	164.33
Pr	24.76	21.54	23.39	24.67	23.61	21.59	23.94	23.06	17.41	25.54	19.83	24.55	14.30	22.15	19.48	17.98	25.69	26.02	20.84
Nd	97.27	87.71	95.01	97.37	92.64	83.39	102.00	90.04	70.38	104.90	82.65	88.33	50.05	81.10	73.74	69.58	100.50	97.89	78.05
Sm	19.35	17.04	17.15	17.96	17.24	16.00	17.94	16.81	14.54	18.98	15.78	15.16	8.19	14.57	13.42	13.39	17.98	16.70	14.33
Eu	4.36	4.00	4.09	4.36	4.14	3.88	4.18	4.11	3.86	4.44	4.10	3.14	2.02	2.99	2.83	3.05	3.90	3.61	3.25
Gd	14.11	12.89	14.14	14.60	14.05	12.78	14.32	13.89	11.41	14.54	12.30	11.95	6.12	10.40	11.00	11.19	13.72	13.48	10.94
Tb	1.79	1.68	1.79	1.87	1.81	1.66	1.83	1.77	1.47	1.76	1.62	1.45	0.72	1.31	1.40	1.48	1.71	1.62	1.31
Dy	8.49	7.94	8.52	8.83	8.44	7.84	8.69	8.22	7.10	8.12	7.86	6.88	3.30	6.06	6.76	7.21	7.85	7.55	5.99
Ho	1.48	1.39	1.47	1.61	1.54	1.42	1.56	1.44	1.23	1.38	1.38	1.26	0.59	1.08	1.26	1.35	1.41	1.38	1.08
Er	3.42	3.24	3.61	3.76	3.60	3.38	3.72	3.54	2.88	3.28	3.22	3.09	1.46	2.66	3.00	3.23	3.40	3.28	2.50
Tm	0.44	0.42	0.47	0.49	0.47	0.44	0.48	0.46	0.36	0.43	0.40	0.40	0.20	0.35	0.41	0.43	0.44	0.43	0.33
Yb	2.51	2.46	2.81	2.88	2.78	2.66	2.84	2.70	2.13	2.45	2.38	2.50	1.21	2.15	2.47	2.63	2.55	2.57	1.97
Lu	0.38	0.35	0.40	0.42	0.41	0.38	0.41	0.40	0.31	0.36	0.35	0.37	0.18	0.32	0.35	0.37	0.37	0.38	0.29
Hf	10.28	9.03	10.08	10.92	10.58	9.09	9.89	9.99	8.00	10.68	9.14	13.61	8.18	11.66	10.83	9.52	12.85	13.55	10.60
Ta	1.98	1.73	1.76	1.73	1.71	1.51	1.77	1.71	1.62	1.55	1.64	1.46	0.96	1.41	1.20	1.26	1.49	1.53	1.39
Tl	0.18	0.14	0.14	0.18	0.15	0.15	0.15	0.14	0.08	0.52	0.55	0.27	0.22	0.22	0.25	0.29	0.19	1.80	0.49
Pb	16.06	13.44	15.05	16.07	15.30	13.54	15.60	16.81	9.69	17.61	13.25	23.52	15.22	19.68	17.18	14.78	18.06	21.62	17.79
Bi	0.22	0.17	0.19	0.18	0.16	0.19	0.20	0.21	0.02	0.21	0.16	0.29	0.05	0.20	0.20	0.18	0.08	0.30	0.25
Th	4.06	3.39	3.86	3.94	3.77	3.59	4.04	3.70	2.63	3.92	2.96	7.65	5.67	8.93	6.41	6.30	4.55	6.21	6.13
U	1.08	0.90	1.07	1.10	1.06	0.90	1.08	1.01	0.75	1.14	0.92	1.72	1.36	2.17	1.34	1.20	1.57	2.00	1.82
Mg#	43.4	42.1	40.0	42.5	42.2	39.8	39.2	40.2	45.8	43.2	42.8	42.2	43.9	36.0	44.3	46.0	30.1	47.5	39.7
Na_2O+K_2O	5.71	5.54	5.72	5.56	5.61	5.62	5.73	5.71	5.88	5.29	4.93	7.58	8.06	7.52	6.75	6.28	6.30	6.34	6.51
K_2O/Na_2O	0.58	0.59	0.62	0.62	0.65	0.62	0.63	0.62	0.57	0.52	0.37	0.98	0.79	0.81	0.72	0.71	0.66	0.80	0.55

Sample number	SB-42BA	SB-44BA	SB-55BA	DG-76BA	GS-82BA	GS-89BA	SB-46BA	SB-57BA	GS-87BA	TU-95BA	KH-14BA	KH-16/1BA	KH-31BA	TU-92BA	KH-36BA	KH-38BA	KH-40BA	SB-50/1BA	SB-50/2BA
Rock type	Basaltic trachyandesite														Trachydacite				
Oxides (wt. %)																			

	SB-50/2BA	SB-50/1BA	KH-40BA	KH-38BA	KH-36BA	TU-92BA	KH-31BA	KH-16/1BA	KH-14BA	TU-95BA	GS-87BA	SB-57BA	SB-46BA	GS-89BA	GS-82BA	DG-76BA	SB-55BA	SB-44BA	SB-42BA
SiO_2	66.98	67.73	63.49	62.97	63.50	51.80	53.85	51.95	52.03	50.59	51.50	51.40	50.92	48.83	52.81	52.58	52.58	53.98	52.79
TiO_2	0.80	0.79	1.09	1.14	1.04	2.56	2.42	2.59	2.83	2.66	2.88	2.58	1.28	2.76	2.65	2.83	2.65	1.35	1.25
Al_2O_3	15.88	15.96	15.61	15.34	15.59	15.24	15.02	15.12	14.77	14.40	14.66	14.28	16.64	15.64	14.76	14.52	14.71	16.69	16.80
Fe_2O_3T	3.13	3.23	5.19	5.83	5.54	9.85	9.64	9.87	11.70	11.32	10.44	10.52	7.94	8.84	9.08	9.85	10.47	7.82	8.58
MnO	0.09	0.1	0.14	0.10	0.10	0.10	0.13	0.22	0.21	0.10	0.12	0.14	0.11	0.09	0.18	0.09	0.10	0.14	0.10
MgO	0.89	0.24	1.12	1.13	0.79	2.56	2.69	2.78	1.93	3.46	2.58	2.97	4.77	4.78	2.41	3.10	3.72	3.69	5.38
CaO	1.24	1.45	2.99	3.26	3.20	7.31	5.60	6.28	6.60	7.54	7.63	7.36	7.52	7.31	7.48	7.32	6.50	6.55	7.42
Na_2O	5.57	5.42	3.85	3.85	3.88	3.63	4.28	3.64	3.62	3.70	3.67	3.63	3.58	4.12	3.48	3.21	3.77	4.05	4.12
K_2O	3.89	4.28	4.80	4.29	4.68	2.18	3.22	3.52	2.91	2.41	2.53	2.34	2.31	2.75	2.58	2.12	2.50	2.62	1.76
P_2O_5	0.17	0.15	0.52	0.57	0.52	1.62	1.43	1.56	1.71	1.40	1.48	1.53	0.62	1.64	1.60	1.74	1.43	0.68	0.43
LOI	1.36	1.08	0.86	1.08	0.68	2.62	1.16	1.94	1.32	1.88	2.08	2.74	3.84	2.34	2.38	2.12	1.08	1.88	0.80
$TOTAL$	100.00	100.44	99.66	99.57	99.52	99.46	99.43	99.46	99.63	99.45	99.56	99.48	99.53	99.09	99.41	99.48	99.51	99.45	99.43
Trace elements (ppm)																			
Li	21.86	20.03	28.03	22.94	23.65	15.73	17.15	18.88	17.91	23.54	30.34	14.53	18.75	12.15	26.89	13.74	12.81	20.83	7.78
Be	2.83	2.87	4.46	4.60	4.65	2.96	3.01	3.50	3.31	2.64	2.77	2.81	1.80	1.45	3.18	2.94	2.85	1.91	1.41
Sc	6.02	5.31	9.88	8.98	7.55	11.85	11.02	15.90	16.29	13.10	12.90	13.49	12.72	11.01	11.28	11.86	14.98	14.40	17.71
V	39.52	36.56	47.80	53.77	45.99	163.69	147.90	167.76	159.95	174.61	178.59	183.75	179.9	163.29	168.99	185.79	179.24	146.7	171.01
Cr	3.27	3.5	11.01	10.43	8.35	67.86	31.00	54.93	48.69	89.85	41.87	48.05	53.67	71.46	47.08	55.11	46.90	59.42	155.95
Co	2.20	1.93	6.83	7.29	5.14	20.81	20.55	23.38	20.20	27.73	23.82	24.77	23.50	24.45	23.86	22.04	23.95	20.45	26.19
Zn	57.59	54.19	135.23	145.87	138.36	158.14	128.95	194.27	161.78	171.00	171.84	174.66	92.55	119.20	172.82	169.09	172.97	106.1	96.26
Ga	21.69	21.76	25.88	26.00	27.10	22.52	24.45	27.07	24.93	22.80	23.23	23.10	20.05	19.59	23.75	23.69	23.38	22.18	21.15
Rb	37.03	85.81	128.75	112.77	93.68	36.61	60.98	116.58	78.92	49.86	48.30	65.50	33.62	35.93	55.52	68.46	53.90	50.20	26.65
Sr	175.17	181.94	559.18	567.62	546.97	1162.7	1176.2	965.94	874.82	949.39	921.67	917.06	1761	3891.9	1001.1	895.99	784.03	1460	1288.10
Y	25.92	22.01	38.48	37.54	34.65	32.80	23.46	38.33	43.25	31.93	33.10	29.63	16.06	12.94	34.96	37.30	30.49	17.89	15.00

Sample number	SB-50/2 BA	SB-50/1B A	KH-40BA	KH-38BA	KH-36BA	TU-92BA	KH-31BA	KH-16/1B A	KH-14BA	TU-95BA	GS-87BA	SB-57BA	SB-46BA	GS-89BA	GS-82BA	DG-76BA	SB-55BA	SB-44BA	SB-42BA
Zr	370.17	390.37	739.04	681.73	704.56	483.83	439.32	614.76	593.22	439.35	448.33	508.70	167.9	155.22	552.44	583.10	488.79	257.4	158.42
Nb	11.85	12.09	35.00	36.98	37.28	29.00	28.55	35.07	32.50	28.81	32.29	31.26	6.65	19.02	33.93	36.14	30.56	9.74	5.53
Cs	2.69	2.84	3.48	3.52	5.54	2.04	0.62	2.06	1.04	4.45	0.66	3.37	0.76	28.38	1.96	1.36	1.00	1.94	0.66
Ba	926.44	1101.3	1795	1670	1795	1552	1575	1481	1421	1230	1107	1101.4	841.6	1633.3	1421	1198.5	1055.8	930.5	671.51
La	28.63	28.94	97.80	92.53	84.73	91.27	95.30	114.32	115.50	76.81	74.78	79.74	39.25	55.03	95.91	98.63	82.89	48.21	29.59
Ce	74.49	51.76	197.2	190.99	182.79	196.68	197.98	238.01	239.89	167.65	163.3	184.2	86.33	114.9	214.3	221.6	179.3	100.8	59.20
Pr	8.56	7.99	26.01	24.68	22.99	24.48	24.66	30.60	31.58	21.16	21.09	23.04	11.54	15.33	26.98	27.73	23.26	13.05	8.20
Nd	35.37	32.28	94.35	91.58	84.85	91.94	90.94	115.72	119.61	82.35	80.56	89.32	43.99	59.23	100.31	106.05	89.60	48.97	32.22
Sm	6.84	0	16.70	17.73	16.25	16.76	15.27	19.89	21.36	16.27	15.92	16.26	7.97	10.82	18.70	19.13	16.17	8.73	6.00
Eu	1.48	1.32	4.08	3.91	4.02	3.60	3.70	4.28	4.50	3.66	3.58	3.61	2.17	3.00	3.89	4.23	3.61	2.36	1.71
Gd	5.82	4.92	13.37	12.14	11.54	12.29	11.65	15.37	16.87	12.01	12.10	12.21	5.98	7.30	13.61	14.92	12.25	6.75	4.74
Tb	0.90	0.75	1.75	1.67	1.54	1.54	1.39	1.92	2.06	1.54	1.56	1.55	0.75	0.79	1.73	1.86	1.57	0.83	0.64
Dy	4.93	4.32	8.90	8.27	7.68	7.36	6.16	9.01	9.70	7.44	7.60	7.28	3.54	3.30	8.18	8.72	7.20	4.04	3.14
Ho	0.99	0.88	1.64	1.50	1.41	1.30	1.00	1.62	1.69	1.33	1.33	1.30	0.65	0.53	1.43	1.53	1.28	0.72	0.59
Er	2.75	2.43	4.01	3.83	3.52	3.14	2.32	3.95	4.30	3.22	3.29	3.01	1.63	1.19	3.48	3.66	3.01	1.79	1.50
Tm	0.42	0.37	0.56	0.53	0.48	0.41	0.28	0.50	0.55	0.42	0.43	0.39	0.24	0.16	0.46	0.48	0.39	0.25	0.22
Yb	2.71	2.45	3.55	3.31	3.08	2.52	1.62	3.01	3.33	2.61	2.58	2.23	1.47	0.90	2.74	2.86	2.26	1.54	1.35
Lu	0.41	0.38	0.51	0.49	0.47	0.38	0.23	0.44	0.49	0.37	0.38	0.32	0.22	0.12	0.40	0.41	0.32	0.24	0.20
Hf	10.12	10.63	18.54	15.95	16.22	10.99	10.28	15.20	14.66	10.20	10.39	11.29	4.46	3.87	12.48	13.06	10.95	6.21	3.98
Ta	0.71	0.73	2.12	2.13	2.13	1.40	1.59	1.80	1.67	1.44	1.74	1.57	0.37	0.81	1.65	1.83	1.57	0.54	0.31
Tl	0.27	0.26	0.71	0.60	0.65	0.43	0.14	0.30	0.24	0.14	0.29	0.24	0.15	0.12	0.37	0.19	0.17	0.18	0.07
Pb	17.55	18.64	29.23	28.81	25.58	18.00	17.71	24.15	29.73	14.50	15.27	17.51	18.74	9.22	19.94	20.07	15.82	18.46	13.09
Bi	0.14	0.14	0.45	0.17	0.21	0.05	0.29	0.31	0.41	0.04	0.04	0.13	0.07	0.03	0.06	0.07	0.11	0.23	0.12
Th	8.57	7.67	13.07	12.55	11.92	4.45	5.00	6.65	6.76	3.61	4.59	4.54	3.43	2.10	5.78	5.20	5.20	4.27	2.56
U	2.25	2.4	3.66	3.66	3.24	1.12	1.36	1.58	1.38	0.93	1.27	1.32	0.81	0.66	1.57	1.58	1.36	1.13	0.52
Mg#	39.9	14.8	33.5	31.1	24.9	37.7	39.4	39.6	27.8	41.6	36.5	39.7	58.3	55.8	38.2	42.3	45.3	52.4	59.4
Na2O+K2O	9.59	9.77	8.75	8.27	8.66	5.99	7.63	7.33	6.64	6.26	6.36	6.16	6.16	7.09	6.24	5.47	6.37	6.84	5.97

Major oxides (wt. %) and trace elements (ppm).

Sample number	K₂O/Na₂O	Rock type	SiO_2	TiO_2	Al_2O_3	Fe_2O_3T	MnO	MgO	CaO	Na_2O	K_2O	P_2O_5	LOI	TOTAL	Li	Be	Sc	V	Cr	Co	Zn	Ga	Rb	Sr	Y	Zr
GS-84BA	0.70	Rhyolite	74.68	0.25	14.09	1.08	0.00	0.29	0.15	4.12	3.97	0.04	1.04	99.70	6.95	1.86	4.51	8.60	2.81	0.77	38.32	16.79	138.21	161.85	34.82	307.37
GS-83BA	0.79		72.55	0.27	15.70	1.17	0.00	0.24	0.17	4.33	4.37	0.05	1.40	100.25	6.09	2.66	4.45	5.69	2.78	0.75	36.86	18.61	143.87	221.73	28.30	324.44
DG-80BA	1.25		74.01	0.27	12.92	1.57	0.02	0.67	0.68	2.19	5.57	0.06	1.82	99.77	25.38	4.31	3.39	16.02	4.29	2.51	34.67	18.10	284.67	82.43	24.26	195.61
DG-74BA	1.11		69.31	1.16	13.76	2.98	0.03	0.63	2.72	3.91	3.85	0.52	1.10	99.96	15.09	3.73	5.84	44.02	4.10	3.96	47.19	20.26	93.00	401.29	22.74	522.96
DO-69BA	1.21		73.89	0.10	14.13	0.67	0.00	0.11	0.50	4.77	4.82	0.02	0.94	99.95	39.29	5.80	3.00	2.21	3.38	0.61	30.96	26.70	160.33	13.24	37.55	336.04
DO-64BA	0.60		70.77	0.57	14.79	2.51	0.04	0.26	0.77	4.72	4.95	0.10	0.76	100.23	20.07	3.52	4.14	18.10	2.95	0.98	61.14	19.04	106.46	107.65	27.08	496.53
DO-61BA	0.75	Rhyolite	72.29	0.35	14.20	1.74	0.03	0.22	0.15	4.60	5.43	0.02	0.72	99.75	12.88	3.46	5.85	8.73	3.47	0.46	63.22	20.85	155.24	15.87	29.13	540.56
SB-49/5BA	0.97		73.50	0.33	13.76	1.70	0.04	0.44	0.32	4.50	4.03	0.10	1.10	99.82	12.31	2.06	2.66	27.33	4.52	2.46	51.38	18.07	65.54	105.86	15.38	219.18
SB-49/3BA	0.80		74.20	0.35	13.65	1.75	0.03	0.45	0.32	4.58	4.03	0.10	1.08	100.54	12.27	1.97	2.74	28.88	4.05	2.29	57.34	18.22	70.84	93.29	17.05	187.34
SB-49/2BA	0.65		73.46	0.34	13.60	2.05	0.04	0.43	0.37	4.74	3.89	0.13	0.94	100.00	10.49	1.91	3.28	23.40	1.86	2.07	58.25	16.78	98.41	141.94	19.02	243.52
SB-49/1BA	0.69		74.01	0.33	13.83	1.77	0.04	0.45	0.34	4.54	4.08	0.10	1.04	100.53	11.40	2.01	2.41	30.20	3.90	2.42	49.64	17.44	48.41	80.14	15.06	177.67
DG-71BA	0.64		68.79	0.60	14.75	3.49	0.04	0.18	1.66	3.88	5.39	0.23	1.10	100.11	9.78	1.97	5.36	27.02	3.09	2.88	46.42	18.22	81.28	219.19	18.83	655.12
DO-68BA	0.64		69.01	0.70	14.66	4.25	0.03	0.51	2.52	4.17	3.24	0.30	1.12	100.51	10.38	2.59	5.58	42.26	49.27	7.89	46.61	20.05	64.01	580.46	14.58	199.94
DO-67BA	0.67		62.33	1.23	16.62	5.44	0.06	0.78	3.08	4.93	3.27	0.45	1.22	99.41	11.15	2.20	9.25	80.84	2.07	7.01	82.87	20.84	63.19	483.12	26.84	343.87
DG-79BA	0.74		64.23	0.98	15.50	4.32	0.06	1.28	1.93	3.58	5.22	0.29	2.66	100.05	20.37	4.08	7.35	41.39	3.52	4.10	95.01	23.30	148.82	213.27	37.78	458.59
DG-78BA	0.66		65.68	0.94	15.57	4.25	0.05	0.56	1.74	4.59	5.20	0.26	0.62	99.47	15.58	3.74	7.52	15.52	1.90	2.51	105.32	21.36	157.59	412.14	41.22	539.79
DO-63BA	0.66	Trachydacite	66.54	0.82	15.66	3.35	0.06	0.76	1.48	4.66	4.92	0.25	1.00	99.49	19.08	3.39	7.62	37.53	2.07	3.10	68.67	20.29	110.14	239.13	30.67	465.05
SB-60BA	0.43	Trachydacite	64.66	1.07	14.92	4.91	0.07	1.53	3.25	3.74	4.32	0.51	0.86	99.84	28.17	3.24	6.05	81.72	26.10	10.50	84.34	21.30	106.78	438.22	18.31	334.12

Oxides in wt. %; trace elements in ppm.

Nb	10.51	11.35	23.11	41.69	26.01	21.97	26.21	11.80	11.94	11.76	11.63	25.45	9.93	13.41	37.92	38.67	21.11	22.93
Cs	4.24	5.97	6.96	1.58	2.55	3.38	3.35	1.12	1.06	1.12	1.10	1.73	2.07	1.43	4.43	10.48	2.82	4.44
Ba	718.35	833.39	427.34	838.02	28.35	1192.40	202.05	733.37	737.48	697.84	721.70	906.18	767.99	1207.41	1492.36	2322.50	1285.01	846.57
La	49.70	52.92	66.59	55.68	49.50	44.55	41.14	24.87	28.36	38.65	22.09	56.17	36.36	50.53	84.48	91.17	58.98	58.95
Ce	141.55	97.78	111.75	112.48	101.14	79.55	65.25	54.79	61.54	62.17	58.73	97.92	65.83	109.33	172.22	146.51	108.60	128.12
Pr	15.69	12.84	14.23	14.08	14.45	11.68	11.21	5.90	6.97	8.25	5.54	12.52	9.18	15.18	20.89	22.95	15.19	14.64
Nd	59.17	48.66	48.59	54.46	55.34	45.60	43.37	21.22	25.41	29.14	19.03	43.29	36.81	59.52	73.29	89.57	57.73	51.83
Sm	10.72	8.76	7.71	9.54	10.80	8.47	7.99	3.44	4.20	4.64	3.40	7.82	6.49	11.66	13.18	15.39	9.97	8.90
Eu	1.47	1.30	0.75	2.22	0.26	1.71	1.40	0.68	0.78	0.84	0.64	1.93	1.58	2.79	2.39	3.71	2.06	1.90
Gd	8.66	7.29	6.02	7.44	8.36	7.12	6.43	2.77	3.35	3.75	2.69	5.54	5.03	9.61	10.38	12.27	8.10	6.48
Tb	1.26	1.03	0.87	1.01	1.36	1.09	1.03	0.43	0.51	0.56	0.43	0.75	0.66	1.30	1.46	1.70	1.16	0.84
Dy	6.68	5.39	4.59	4.97	7.86	5.78	5.91	2.62	2.88	3.12	2.73	3.80	3.14	6.41	7.66	8.85	6.14	4.01
Ho	1.34	1.06	0.90	0.91	1.59	1.13	1.18	0.56	0.61	0.66	0.56	0.72	0.56	1.16	1.45	1.62	1.19	0.72
Er	3.54	2.83	2.48	2.24	4.33	2.94	3.27	1.76	1.80	1.94	1.65	1.93	1.42	2.87	3.71	4.04	3.09	1.82
Tm	0.52	0.42	0.38	0.32	0.66	0.43	0.49	0.29	0.29	0.33	0.27	0.29	0.20	0.39	0.52	0.54	0.45	0.26
Yb	3.29	2.78	2.55	1.92	4.36	2.74	3.29	2.04	2.02	2.24	1.94	1.86	1.25	2.33	3.25	3.31	2.94	1.64
Lu	0.51	0.43	0.38	0.30	0.64	0.41	0.50	0.33	0.32	0.36	0.30	0.29	0.18	0.34	0.48	0.48	0.45	0.24
Hf	8.76	9.39	5.94	12.74	11.19	12.37	14.71	6.13	5.38	6.58	4.92	14.60	5.19	9.13	11.84	12.90	11.49	8.60
Ta	0.75	0.78	1.86	2.57	1.88	1.33	1.62	0.90	0.91	0.84	0.87	1.44	0.71	0.80	2.20	2.15	1.26	1.59
Tl	0.85	0.88	1.49	0.11	0.95	0.68	0.56	0.31	0.30	0.29	0.29	0.21	0.20	0.32	0.80	0.62	0.61	0.82
Pb	14.88	15.91	28.13	14.70	23.94	21.14	21.13	15.47	14.07	15.76	13.30	13.11	17.66	18.21	26.58	24.45	19.38	16.76
Bi	0.04	0.04	0.07	0.04	0.08	0.12	0.12	0.09	0.07	0.04	0.08	0.03	0.06	0.09	0.10	0.06	0.07	0.17
Th	14.66	14.49	34.77	11.22	16.14	11.32	16.28	11.26	12.03	11.87	10.88	7.59	8.03	7.49	18.52	14.40	12.25	18.04
U	3.41	2.51	3.59	1.73	2.58	2.43	3.37	2.31	2.47	2.10	2.26	2.16	1.98	1.28	3.95	1.82	1.98	3.94
Mg#	38.5	32.3	49.9	33.0	27.7	19.4	22.8	37.6	37.5	32.8	37.2	10.7	21.9	25.0	40.8	23.5	34.6	42.1
Na₂O+K₂O	8.19	8.80	7.92	7.84	9.68	9.72	10.13	8.64	8.66	8.72	8.66	9.36	7.45	8.36	9.04	9.91	9.73	8.14
K₂O/Na₂O	0.96	1.01	2.54	0.99	1.01	1.05	1.18	0.90	0.88	0.82	0.90	1.39	0.78	0.66	1.46	1.13	1.06	1.16

References

Avanzinelli, R., Lustrino, M., Mattei, M., Conticelli, S., 2009. Potassic and ultrapotassic magmatism in the Circum-Tyrrhenian region: Significance of carbonated pelitic vs. pelitic sediment recycling at destructive plate margins. Lithos 113, 213-227.

Ayers, J., Dittmer, S. and Layne, G., 1997. Partitioning of elements between peridotite and H2O at 2.0-3.0 Gpa and 900-1100C, and application to models of subductions zone processes. Earth and Planetary Science Letters, 381-398.

Badarch, G., Cunningham, D.W. and Windley, B.F., 2002. A new terrane subdivision for Mongolia: implications for the Phanerozoic crustal growth of Central Asia. Journal of Asian Earth Sciences 21, 87-110.

Chakrabarti, R., Basu, A.R., Santo, A.P., Tedesco, D. and Vaselli, O., 2009. Isotopic and geochemical evidence for a heterogeneous mantle plume origin of the Virunga volcanics, Western rift, and East African Rift system. Journal of Chemical Geology 259, 273-289.

Chambell, I.H., Stepanov, A.S., Liang, H.Y., Allen, C.M., Norman, M.D., Zhang, Y.Q. and Xie, Y.W., 2014. The origin of shoshonites: new insights from the Tertiary high-potassium intrusions of eastern Tibet. Mineral Petrol 167, 983.

Chen, Y., Zhang, Y., Graham, D., Su, S. and Deng, J., 2007. Geochemistry of Cenozoic basalts and mantle xenolith in Northeast China. Lithos 96, 108-126.

Chuvashova, I., Rasskazov, S. and Yasnygina, T., 2016. Mid-Miocene thermal impact on the lithosphere by sub-lithospheric convective mantle material: Transition from high- to moderate-Mg magmatism beneath Vitim Plateau, Siberia. Geoscience Frontiers, 1-22.

Cogné, J.P., Kravchinsky, V.A., Halim, N. and Hankard, F., 2005. Late Jurassic-Early Cretaceous closure of the Mongol-Okhotsk Ocean demonstrated by new Mesozoic paleomagnetic results from the Trans-Baïkal area (SE Siberia). Geophysical Journal International 163, 813-832.

Condie, K.C, 2005. High field strength element ratios in Archean basalts: a window to evolving sources of mantle plumes? Lithos 79, 491-504.

Conticelli, S., Guarnieri, L., Farinelli, A., Mattei, M., Avanzinelli, R., Bianchini, G., Boari, B.,Tommasini, S., Tiepolo, M., Prelević, D. and Venturelli, G., 2009. Trace elements and Sr–Nd–Pb isotopes of K-rich, shoshonitic, and calc-alkaline magmatism of the Western Mediterranean Region: Genesis of ultrapotassic to calc-alkaline magmatic associations in a post-collisional geodynamic setting. Lithos 107, 68-92.

Dash, B., Yin, A., Jiang, N., Tseveendorj, B. and Han, B., 2013. Petrology, structural setting, timing, and geochemistry of Cretaceous volcanic rocks in eastern Mongolia: Constraints on their tectonic origin. Gondwana Research 27, 281-299.

Dong, Y., Ge, W.C., Yang, H., Zhao, G., Wang, Q., Zhang, Y. and Su, L., 2014. Geochronology and geochemistry of Early Cretaceous volcanic rocks from the Baiyingaolao Formation in the central Great Xing'an Range, NE China, and its tectonic implications. Lithos 205, 168-184.

Donskaya, T.V., Gladkochub, D.P., Mazukabzov, A.M. and Ivanov, A.V., 2013. Late Paleozoic – Mesozoic subduction-related magmatism at the southern margin of the Siberian continent and the 150 million-year history of the Mongol-Okhotsk Ocean. Journal of Asian Earth Sciences 62, 79-97.

Donskaya, T.V., Gladkochub, D.P., Mazukabzov, A.M., Waele, B.D. and Presnyakov, S.L., 2012. The Late Triassic Kataev volcano plutonic association in western Transbaikalia, a fragment of the active continental margin of the Mongol-Okhotsk Ocean. Russian Geology and Geophysics 53, 22–36.

Duraiswami, R.A. and Shaikh, T.N., 2013. Geology of the saucer-shaped sill near Mahad, western Deccan Traps, India, and its significance to the Flood Basalt Model. Bulletin of Volcanology 75, 1-18.

Fan, W.M., Guo, F., Wang, Y.J., Lin, G., 2003. Late Mesozoic calc-alkaline volcanism of post-orogenic extension in the northern Da Hinggan Mountains, northeastern China. Journal of Volcanology and Geothermal

Research 121, 115-135.

Faure, M. and Natal'in, B., 1992. The geodynamic evolution of the eastern Eurasian margin in Mesozoic times. Journal of Tectonophysics 208, 397-411.

Fitton, J.G. and Godard, M., 2004. Origin and evolution of magmas on the Ontong Java Plateau. Geological Society, London-Special Publications 229, 151-178.

Gao, Y, 2008. Chronology and Geochemistry of Mesozoic volcanic rocks in Southern Songliao Basin. Master Dissertation. Jilin University, 1-78.

Ge, W.C., Chen, J.S., Yang, H., Zhao, G.C., Zhang, Y.L. and Tian, D.X., 2015. Tectonic implications of new zircon U–Pb ages for the Xinghuadukou Complex, Erguna Massif, and northern Great Xing'an Range, NE China. Journal of Asian Earth Sciences 106, 169-185.

Ge, W.C., Lin, Q., Sun, D.Y., Wu, F.Y., Yuan, Z.K., Li, W.Y., Chen, M.Z. and Yin, C.X., 1999. Geochemical characteristcs of the Mesozoic basalts in Da Hinggan Ling: evidence of the mantle-crust interaction. Acta Petrol. Sin. 15, 397-407. (In Chinese).

Genc, S.C and Tuysuz, O, 2010. Tectonic setting of the Jurassic bimodal magmatism in the Sakarya Zone (Central and Western Pontides), Northern Turkey: a geochemical and isotopic approach. Lithos.

Graham, S.A., Hendrix, M.S., Johnson, C.L., Badarch, G., Amory, J., Porter, M., Basrbold, R., Webb, L.E. and Hacker, B.R., 2001. Sedimentary record and tectonic implications of Mesozoic rifting in southeast Mongolia. GSA Bulletin 12, 1560-1579.

Grebennikov, A.V., Khanchuk A.I., Gonevchuk, V.G. and Kovalenko S.V., 2016. Cretaceous and Paleogene granitoid suites of the Sikhote-Alin area (Far East Russia): Geochemistry and tectonic implications. Lithos 261, 250-261.

Guo, F., Fan, W., Gao, X. and Li, H., 2010. Sr–Nd–Pb isotope mapping of Mesozoic igneous rocks in NE China: Constraints on tectonic framework and Phanerozoic crustal growth. Lithos 120, 563-578.

Guo, F., Fan, W., Li, C., Gao, X., Miao, L., 2008. Early Cretaceous highly positive εNd felsic volcanic rocks from the Hinggan Mountains, NE China: origin and implications for Phanerozoic crustal growth. Journal of Earth Sciences 98, 1395-1411.

Guo, J., Guo, F., Yan Wang, C.Y. and Li, C., 2013. Crustal recycling processes in generating the early Cretaceous Fang cheng basalts, North China Craton: New constraints from mineral chemistry, oxygen isotopes of olivine and whole-rock geochemistry. Lithos 170-171, 1-16.

Guo, S., Evans, D.G. and Li, D., 2006. Preparation of C.I. Pigment 52:1 anion-pillared layered double hydroxide and the thermo- and photostability of the resulting intercalated material. Journal of Physics and Chemistry of Solids 67, 1002-1006.

Institute of Geology, Ministry of Heavy industry of Mongolia, 1990. Geological Map of Mongolia; 1:500 000 scale.

Jahn, B.M., Valui, G., Kruk, N., Gonevchuk, V., Usuki, M. and Jeremy, T.J.W., 2015. Emplacement ages, geochemical and Sr–Nd–Hf isotopic characterization of Mesozoic to early Cenozoic granitoids of the Sikhote-Alin Orogenic Belt, Russian Far East: Crustal growth and regional tectonic evolution. Journal of Asian Earth Sciences 111, 872-918.

Jahn, B.M., Litvinovsky, B.A., Zanvilevich, A.N. and Reichow, M.K., 2009. Peralkaline granitoid magmatism in the Mongolian–Transbaikalian Belt: Evolution, petrogenesis and tectonic significance. Lithos 113, 521-539.

Jahn, B.M, 2004. The Central Asian Orogenic Belt and growth of the continental crust in the Phanerozoic. In Malpas J. Fletcher C. J. N. Ali J. R. & Aitchison J. C. (eds). Aspects of the Tectonic Evolution of China. 226, 73–100. Geological Society of London, Special Publication.

Jahn, B.M., Wu, F.Y. and Chen, B., 2000. Massive granitoid generation in central Asia: Nd isotopic evidence and implication for continental growth in the Phanerozoic. Episodes 23, 82–92.

Ji W., Xu W., Yang, D., Pei, F., Jin, K. and Liu, X., 2007. Chronology and Geochemistry of Volcanic Rocks in the Cretaceous Suifenhe Formation in Eastern Heilongjiang, China.

Acta Geologica Sinica - English Edition 81, 266-277.

Karsli, O., Dokuz, A., Kaliwoda, M., Uysal, I., Aydin, F., Kandemir, R. and Fehr, K.T., 2014. Geochemical fingerprints of Late Triassic calc-alkaline lamprophyres from the Eastern Pontides, NE Turkey: A key to understanding lamprophyre formation in a subduction-related environment. Lithos 196–197, 181-197.

Kessel, R., M. W. Schmidt, P. Ulmer, and T. Pettke., 2005. Trace element signature of subduction-zone fluids, melts and supercritical liquids at 120–180 km depth, Nature 437, 724–727.

Kojima, S., 1989. Mesozoic terrane accretion in Northeast China, Sikhote-Alin and Japan regions. Palaeo geography, Palaeo climatology, Palaeoecology 69, 213-232.

Kravchinsky, V.A., Cogne, J.P., Harbert, W.P. and Kuzmin, M.I., 2002. Evolution of the Mongol–Okhotsk Ocean as constrained by new palaeomagnetic data from the Mongol–Okhotsk suture zone, Siberia. Journal of Geophys 148, 34–57.

Labanieh, S., C. Chauvel, A. Germa, and X. Auidelleur (2012), Martinique: function of distance to the trench, J. Petrol 53, 2441–2464.

Li, Y., Ma, C.Q., Xing, G.F., Zhou, H.W., 2015. The Early Cretaceous evolution of SE China: insights from the Changle–Nan'ao Metamorphic Belt. Lithos 230, 94–104.

Li, S.C., Liu, Z.H., Xu, Z.Y., Li, G. and Zhang, C., 2014. Age and tectonic setting of volcanic rocks of the Tamulangou Formation in the Great Xing'an Range, NE China. Journal of Asian Earth Sciences 113, 471-480.

Li, S.Q., Hegner, E., Yang, Y.Z., Wu, J.D. and Chen, F., 2014. Age constraints on late Mesozoic lithospheric extension and origin of bimodal volcanic rocks from the Hailar basin, NE China. Lithos 190-191, 204-219.

Li, S., Mooney, W.D. and Fan, J., 2006. Crustal structure of mainland China from deep seismic sounding data. Tectonophysics 420, 239-252.

Li, J. and Shu, L, 2002. Mesozoic_Cenozoic Tectonic Features and Evolution of the Songliao Basin, NE China. Journal of Nanjing University, Natural Sciences 38, 525-531. (In Chinese with English abstract).

Liu, Y.J., Li, W.M., Zhiqiang, F. and Liang, C., 2016. A review of the Paleozoic tectonics in the eastern part of Central Asian Orogenic Belt. Gondwana Research 01606, 1-26.

MacDonald, R., Rogers, N.W., Fitton, J.G., Black, S. and Smith, M., 2001. Plume–Lithosphere Interactions in the Generation of the Basalts of the Kenya Rift, East Africa. Journal of Petrology 42, 877-900.

Maitre. R.W.L., Bateman, P., Dudek, A., Keller, J., Lameyre, J.. Le Bas, M.J., Sabine, P.A., Schmid, R., Sorensen, H., Streckeisen, A., Woolley, A.R. and Zanettin, B., 1989. A Classification of Igneous Rocks and Glossary of terms: Recommendations of the International Union of Geological Sciences Subcommission on the Systematics of Igneous Rocks. Blackwell Scientific Publications, Oxford, U.K.

Meng, E., Xu, W.L., Yang, D.B., Qiu, K.F., Li, C.H. and Zhu, H.T., 2011. Zircon U-Pb chronology, Geochemistry of Mesozoic volcanic rocks from the Lingquan basin in Manzhouli area, and its tectonic implications. Acta Petrologica Sinica 27, 1209-1226. (In Chinese with English abstract).

Meng, Q.-R., 2003. What drove late Mesozoic extension of the northern China–Mongolia tract? Journal of Tectonophysics 369, 155-174.

Miao, L., Zhang, F.Q., Zhu, M.S. and Liu D.Y., 2015. Zircon SHRIMP U–Pb dating of metamorphic complexes in the conjunction of the Greater and Lesser Xing'an ranges, NE China: Timing of formation and metamorphism and tectonic implications. Journal of Asian Earth Sciences 114, 634-648.

Miao, L., Fan, W., Liu, D., Zhang, F., Shi, Y. and Guo, F., 2008. Geochronology and geochemistry of the Hegenshan ophiolitic complex: Implications for late-stage tectonic evolution of the Inner Mongolia-Daxinganling Orogenic Belt, China. Asian Earth Sciences 32, 348–370.

Miao, L., Liu D.Y., Zhang, F.Q., Fan, W.M., Shi, Y.R. and Xie, H.Q., 2007. Zircon SHRIMP U-Pb ages of the "Xinghuadukou Group" in Hanjiayuanzi and Xinlin areas and the "Zhalantun Group" in Inner Mongolia, Da

Hinggan Mountains. Chinese Science Bulletin 52, 1112–1124.

Miao, L., Fan, W., Zhang, F., Liu, D., Jian, P., Shi, G., Tao, H. and Shi, Y., 2004. Zircon SHRIMP geochronology of the Xinkailing-Kele complex in the northwestern Lesser Xing'an Range,and its geological implications. Chinese Science Bulletin 49, 201-209.

Niu, Y., Liu, Y., Xue, Q., Shao, F., Chen, S., Duan, M., Guo, P., Gong, H., Hu, Y., Hu, Z., Kong, J., Li, J., Liu, J., Sun, P., Sun, W., Ye, L., Xiao, Y. and Zhang, Y., 2015. Exotic origin of the Chinese continental shelf: new insights into the tectonic evolution of the western Pacific and eastern China since the Mesozoic. Science Bulletin 60, 1598-1616.

Nivia, A., Marriner, G.F., Kerr, A.C. and Tarney, J., 2006. The Quebradagrande Complex: A Lower Cretaceous ensialic marginal basin in the Central Cordillera of the Colombian Andes. Journal of South American Earth Sciences 21, 423-436.

Pearce, J. A., Stern, R. J., Bloomer, S. H. and P. Fryer, 2005. Geochemical mapping of the Mariana arc-basin system: Implications for the nature and distribution of subduction components, Geochem. Geophys 6.

Pearce, J.A, 1983. Role of the sub-continental lithosphere in magma genesis at active continental margins. Continental Basalts and Mantle Xenoliths, 230-249.

Pearce, J.L and Stern, R.J, 2006. Origin of Back-Arc basin magmas: Trace element and isotope perspectives, in Back Arc Spreading Systems: Geological, Biological, Chemical, and Physical Interactions, edited by D. M. Christie et al., 63–86, Geophysical Monograph Series, Washington, D.C.

Peccerillo, A., Taylor, S.R., 1976. Geochemistry of Eocene calc-alkaline volcanic rocks from the Kastamonu area, Northern Turkey. Contributions to Mineralogy and Petrology 58, 63–81.

Safonova, I., Kojima, S., Nakae, S., Romer, R.L., Seltmann, R., Sano, H. and Onoue, T., 2015. Oceanic island basalts in accretionary complexes of SW Japan: Tectonic and petrogenetic implications. Journal of Asian Earth Sciences 113, 508-523.

Sato, D., Matsuura, H. and Yamamoto, T., 2016. Timing of the Late Cretaceous ignimbrite flare-up at the eastern margin of the Eurasian Plate: New zircon U-Pb ages from the Aioi-Arima-Koto region of SW Japan. Journal of Volcanology and Geothermal Research, Volume 310, 89-97.

Şengör, A.M.C. and Natal'in, B.A., 1996. Paleotectonics of Asia: fragments of a synthesis, in Yin, A. and Harrison, M., eds., and the tectonic evolution of Asia: New York, Cambridge Univercity Press, 486-640.

Şengör, A.M.C., Natal'in, B.A. and Burtman, V.S., 1993. Evolution of the Altaid tectonic collage and Palaeozoic crustal growth in Eurasia. Nature 364: 299-307.

Shu, P., Ding, R.X., Ji, X.Y. and Qu, Y.M., 2007. SHRIMP zircon geochronology of reservoir volcanic rocks in the Qingshen gas field, Songliao Basin. Acta petrologica et Mineralogica 26, 239-246. (In Chinese with English abstract).

Shuvalov, V.F, 1982. Mezozoiskie ozernye basseiye Mongolii, in Martinson, G.G ed., Limnobois drevnikh ozernykh basseinov Evrazii: Nauka Leningrad, 18-80.

Shuvalov, V.F, 1980. Jurskie I nizhnemelovye Vostochnoy Gobi I raspredelenie v nikh iskopaemoy fauny I flory, in Martinson, G.G., ed., Limnobois drevnikh ozernykh basseinov Evrazii: Nauka Leningrad, 91-118.

Stern, R.J., Fouch, M.J., and Klemerer, S.L., 2003. An overview of the Izu-Bonin-Mariana subduction factory, in Eiler, J., ed., inside the subduction duction factory: American Geophysical Union Geophysical Monograph 138, 175–221.

Sun, M.D., Chen, H.L., Zhang, F.Q., Wilde, S.A., Dong, C.W. and Yang, S.F., 2013. A 100 Ma bimodal composite dyke complex in the Jiamusi Block, NE China: An indication for lithospheric extension driven by Paleo-Pacific roll-back. Lithos 162-163, 317-330.

Svetlitskaya, T.V. and Nevolko, P.A., 2016. Late Permian–Early Triassic traps of the Kuznetsk Basin, Russia: Geochemistry and petrogenesis in respect to an extension of the Siberian Large Igneous Province. Gondwana Research 39, 57-76.

Tomurtogoo, O., Gantumur, H. and Zul, B., 2012. Geological Map of Northern-Central-Eastern Asia and Adjacent areas, 1: 2 500 000 scale.

Van der Voo, R., Spakman, W. and Bijwaard, H., 1999. Mesozoic subducted slabs under Siberia. Nature 397, 246-249.

Wang, F., Zhou, X.H., Zhang, L.C., Ying, J.F., Zhang, Y.T., Wu, F.Y. and Zhu, R.X., 2006. Late Mesozoic volcanism in the Great Xing'an Range (NE China): Timing and implications for the dynamic setting of NE Asia. Earth and Planetary Science Letters 251, 179-198.

Wang, Y., Fan, W. and Guo, F., 2002. K-Ar dating of late Mesozoic volcanism and geochemistry of volcanic gravels in the North Huaiyang Belt, Dabie orogen: Constraints on the stratigraphic framework and exhumation of the northern Dabie orthogneiss complex. Chinese Science Bulletin 47, 1688-1695.

Windley, B.F., Alexeiev, D., Xiao, W., Kroner, A. and Badarch, G., 2007. Tectonic models for accretion of the Central Asian Orogenic Belt. Journal of the Geological Society 164, 31-47.

Wu, F.Y., Lin, J,Q., Wilde, S.A., Zhang, X.O. and Yang, J.H., 2005a. Nature and significance of the Early Cretaceous gaint igneous event in eastern China. Earth Planet. Sci. Lett 233, 103-119.

Wu, F.Y., Sun, D.Y., Ge, W.C., Zhang, Y.B., Grant, M.L., Wilde, S.A. and Jahn, B.M., 2011. Geochronology of the Phanerozoic granitoids in northeastern China. Journal of Asian Earth Sciences 41, 1-30.

Wu, G., Sun, F.Y., Zhao, C.S., Li, Z.T., Zhao, A.L., Pang, Q.B., Li, G.Y., 2005. Discovery of the Early Paleozoic post-collisional granites in northern margin of the Erguna massif and its geological significance. Chin. Sci. Bull 50, 2733–2743.

Xiao, W., Huang, B., Han, C., Sun, S. and Li, J., 2010. A review of the western part of the Altaids: A key to understanding the architecture of accretionary orogens. Journal of Gondwana Research, 18, 253-273.

Xiao, W.J., Windley, B.F., Hao, J., Zhai, M.G., 2003. Accretion leading to collision and the Permian Solonker suture, Inner Mongolia, China: termination of the central Asian orogenic belt. Tectonics 22, 10.

Xu, W.L., Pei, F.P., Wang, F., Meng, E., Ji, W.Q., Yang, D.B. and Wang, W., 2013. Spatial–temporal relationships of Mesozoic volcanic rocks in NE China: Constraints on tectonic overprinting and transformations between multiple tectonic regimes. Journal of Asian Earth Sciences 74, 167-193.

Yang, S., Miao, L., Zhang, F., Meng, Q., Zhu, M., Munkhtsengel, B. and Chimedtseren, A., 2016. Zircon age and geochemistry of the Tost bimodal volcanic rocks: Constraints on the Early Carboniferous tectonic evolution of the South Mongolia. Journal of Asian Earth Sciences 120, 29-42.

Yang, W.B., Niu, H.C., Cheng, L.R., Shan, Q. and Li, N.B., 2015. Geochronology, geochemistry and geodynamic implications of the Late Mesozoic volcanic rocks in the southern Great Xing'an Mountains, NE China. Journal of Asian Earth Sciences 113, 454-470.

Yang, Y.T., Guo, Z.X., Song, C.C. and He, X.B.L., 2014. A short-lived but significant Mongol–Okhotsk collisional orogeny in latest Jurassic–earliest Cretaceous. Gondwana Research. 1-21.

Yarmolyuk, V.V., Kudryashova, E.A., Kozlovsky, A.M., Lebedev, V.A. and Savatenkov, V.M., 2015. Late Mesozoic–Cenozoic Intraplate Magmatism in Central Asia and Its Relation with Mantle Diapirism: Evidence from the South Khangai Volcanic Region, Mongolia. Asian Earth Sciences.

Ying, J.F., Zhou, X.H., Zhang, L.C., Wang, F., 2010. Geochronological framework of Mesozoic volcanic rocks in the Great Xing'an Range, NE China, and their geodynamic implications. Journal of Asian Earth Sciences 39, 786–793.

Yu, Y., Xu, W., Pei, F., Yang, D. and Zhao, Q., 2009. Chronology and Geochemistry of Mesozoic Volcanic Rocks in the Linjiang area, Jilin Province and their tectonic implications. Acta Geologica Sinica 83, 245-257.

Zhang, F.Q., Chen, H.L.,Yu, X., Dong, C.W., Yang, S.F., Pang, Y.M. and Batt, G.E., 2011. Early Cretaceous volcanism in northern Songliao Basin, NE China, and its geodynamic implication. Gondwana Research 19, 163-176.

Zhang, F.Q., Chen, H.L., Dong, C.W., Pang, Y.M.,

Shu, P., Wang, Y.L., Yang, S.F., 2008. SHRIMP zircon U–Pb geochronology of volcanic rocks and discussion on the geological time of the Yingcheng Formation of the northern Songliao basin. Journal of Stratigraphy 32, 15–20 (in Chinese with English abstract).

Zhang, H.F., Nakamura, E., Sun, M., Kobayashi, K., Zhang, J., Ying, J.F., Tang, Y.J. and Niu, L.F., 2007. Transformation of subcontinental lithospheric mantle through peridotite-melt reaction: evidence from a higjly fertile mantle xenolith from the North China Craton. International Geology Review 49, 658-679.

Zhang, J.H., Gao, S., Ge, W.C., Wu, F.Y., Yang, J.H., Wilde, S.A. and Li, M., 2010. Geochronology of the Mesozoic volcanic rocks in the Great Xing'an Range, northeastern China: Implications for subduction-induced delamination. Chemical Geology 276, 144-165.

Zhang, J.H., Ge, W.C., Wu, F.Y., Wilde, S.A., Yang, J.H., Liu, X.M., 2008. Large-scale early Cretaceous volcanic events in the northern Great Xing'an Range, Northeastern China. Lithos 102, 138–157.

Zhang, L.C., Zhou, X.H., Ying, J.F., Wang, F., Guo, F., Wan, B. and Chen, Z.G., 2008. Geochemistry and Sr–Nd–Pb–Hf isotopes of Early Cretaceous basalts from the Great Xinggan Range, NE China: Implications for their origin and mantle source characteristics. Chemical Geology 256, 12-23.

Zhao, G.L., Yang, G.L., Wang, Z., Fu, J.F., Yang, Y.Z., 1989. Mesozoic Volcanic Rocks in Middle–South Da-Hinggan Mountains. Beijing Science and Technology Publishing House, Beijing, 252. (In Chinese).

Zhou, J.B., Cao, J.L., Wilde, S.A., Zhao, G.C., Zhang, J.J. and Wang, B., 2014. Paleo-Pacific subduction-accretion: Evidence from Geochemical and U-Pb zircon dating of the Nadanhada accretionary complex, NE China. Tectonics 33, 2444-2466.

Zhou, J.B., Wilde, S.A., Zhang, X.Z., Ren, S.M. and Zheng, C.Q., 2011a. Early Paleozoic metamorphic rocks of the Erguna block in the Great Xing'an Range, NE China: Evidence for the timing of magmatic and metamorphic events and their tectonic implications. Tectonophysics 499, 105-117.

Zorin, Y.A., 1999. Geodynamics of the western part of the Mongolia–Okhotsk collisional belt, Trans-Baikal region (Russia) and Mongolia. Tectonophysics 306, 33-56.